Cell Reports

Article

Acid-adapted cancer cells alkalinize their cytoplasm by degrading the acid-loading membrane transporter anion exchanger 2, *SLC4A2*

Graphical abstract

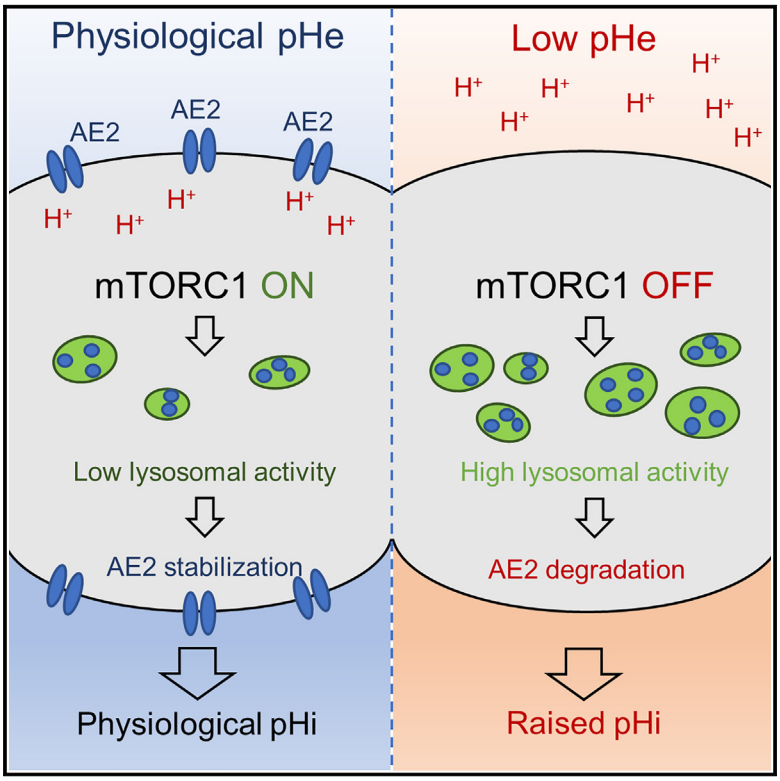

Authors

Johanna Michl, Stefania Monterisi, Bobby White, ..., Zinan Yin, Walter F. Bodmer, Pawel Swietach

Correspondence

pawel.swietach@dpag.ox.ac.uk

In brief

It remains unclear how cancer cells can maintain a physiological intracellular pH, despite their acidic microenvironment. Michl et al. show that extracellular acidity triggers the lysosomal degradation of anion exchanger 2 (AE2), an acid-loading membrane transporter. Reduced AE2 activity raises intracellular pH toward physiological levels in cells under chronic acidosis.

Highlights

- Screen of 66 cancer cell lines reveals variation in pHi-regulatory phenotypes
- Resting pHi is set by the activity of acid-loading anion exchanger 2 (AE2)
- Cancer cells adapt to acidic environments by degrading AE2, which raises pHi
- Lysosomal degradation of AE2 is triggered by mTORC1 inhibition by low pHi

Michl et al., 2023, Cell Reports *42*, 112601
June 27, 2023
https://doi.org/10.1016/j.celrep.2023.112601

CellPress

Cell Reports

CellPress
OPEN ACCESS

Article

Acid-adapted cancer cells alkalinize their cytoplasm by degrading the acid-loading membrane transporter anion exchanger 2, *SLC4A2*

Johanna Michl,[1] Stefania Monterisi,[1] Bobby White,[1] Wiktoria Blaszczak,[1] Alzbeta Hulikova,[1] Gulnar Abdullayeva,[2] Esther Bridges,[3] Zinan Yin,[3] Walter F. Bodmer,[2] and Pawel Swietach[1,4,*]

[1]Department of Physiology, Anatomy and Genetics, Parks Road, Oxford OX1 3PT, UK
[2]MRC Weatherall Institute for Molecular Medicine, John Radcliffe Hospital, Headington, Oxford OX3 9DS, UK
[3]Department of NDM Experimental Medicine, MRC Human Immunology Unit, MRC Weatherall Institute of Molecular Medicine, JR Hospital, Headington, Oxford OX3 9DS, UK
[4]Lead contact
*Correspondence: pawel.swietach@dpag.ox.ac.uk
https://doi.org/10.1016/j.celrep.2023.112601

SUMMARY

Acidic environments reduce the intracellular pH (pHi) of most cells to levels that are sub-optimal for growth and cellular functions. Yet, cancers maintain an alkaline cytoplasm despite low extracellular pH (pHe). Raised pHi is thought to be beneficial for tumor progression and invasiveness. However, the transport mechanisms underpinning this adaptation have not been studied systematically. Here, we characterize the pHe-pHi relationship in 66 colorectal cancer cell lines and identify the acid-loading anion exchanger 2 (AE2, *SLC4A2*) as a regulator of resting pHi. Cells adapt to chronic extracellular acidosis by degrading AE2 protein, which raises pHi and reduces acid sensitivity of growth. Acidity inhibits mTOR signaling, which stimulates lysosomal function and AE2 degradation, a process reversed by bafilomycin A1. We identify AE2 degradation as a mechanism for maintaining a conducive pHi in tumors. As an adaptive mechanism, inhibiting lysosomal degradation of AE2 is a potential therapeutic target.

INTRODUCTION

Increased acid production and impaired capillary washout produce an acidic tumor microenvironment.[1–3] Considering thermodynamic constraints, such conditions should reduce the intracellular pH (pHi). If uncorrected, this would impose unfavorable consequences on cancer cells because many biological functions are suppressed at low pHi.[4–6] Studies of aggressive cancers provided *in vivo* evidence for alkaline intracellular conditions despite low extracellular pH (pHe),[7,8] indicating that tumors overcome the aforementioned challenge. Raised pHi is considered necessary for cancer progression because it is permissive for proliferation, evading death, invasiveness, and migration.[9–14] Furthermore, certain gain-of-function mutations exploit pHi sensitivity. For instance, the R237H substitution in the tumor suppressor p53 reduces DNA binding at raised pHi.[15,16]

A mechanism for raising pHi in cancer cells would offer a survival advantage under acid stress. However, its identity remains unknown, not least because of inconsistent data quality. Accurate pHi measurements pose multiple challenges; for example, those carried out on tissues lack single-cell resolution. Some *in vitro* recordings have used inappropriate buffering conditions.[17] For instance, the use of bicarbonate-free buffers can lead to flawed estimates of resting pHi because HCO_3^--dependent transporters become inactivated.[17–19] Another cause of concern relates to CO_2 stability while transferring cells from incubators (5%–10% CO_2) to CO_2-free measurement devices, which inevitably overestimates pHi. Moreover, pHi must be reported in the context of pHe since the two are coupled.[17] Without accurate reporting standards, it has been difficult to identify the transport process underpinning acid adaptation.

Several studies have described how H^+ ions can be redistributed within a cell by means of acid (or base) sequestration into organelles, such as lysosomes[20] or the Golgi apparatus.[21] However, these organelles have finite volume and buffering, and when faced with a continuous source of acid (like metabolism), their capacity to take up excess acid is saturable, unless a secondary process expunges their contents (e.g., exocytosis). In this sense, the act of pHi regulation is performed by the exocytotic event, which is complex and resource intensive. The most direct mechanism for stably alkalizing cells under a continuous (e.g., metabolic) source of acid involves the transport of H^+ equivalents across the plasma membrane. Surface-expressed transporters are the gatekeepers of pHi because they export excess acid (or base) into the extracellular space, which is essentially infinite *in vivo* (due to perfusion) and *in vitro* (due to large extracellular volumes or superfusion). Rightly, many studies of pHi regulation have focused on the role of ion transporters at the cell surface, such as Na^+/H^+ exchanger 1 (*SLC9A1*, NHE1), monocarboxylate transporter 1

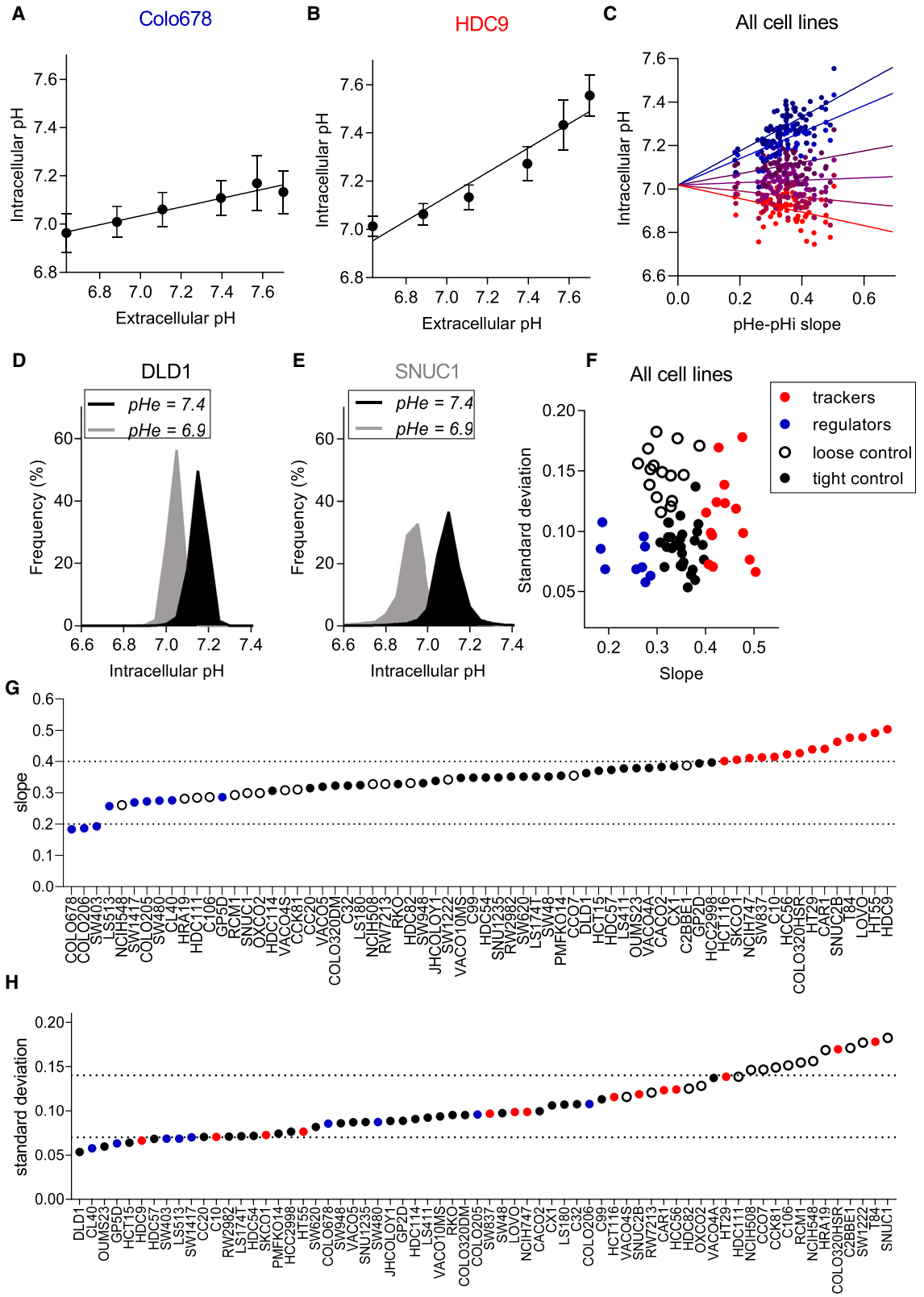

(legend on next page)

(*SLC16A1*, MCT1),[1,22,23] and Na^+/HCO_3^- co-transporters (NBCs that import HCO_3^-, the chemical equivalent of H^+ extrusion).[24,25] In the context of pHi regulation in tumors, emphasis on acid-extruding mechanisms is intuitive because cancer cells are net acid producers. Inadvertently, less attention has been given to acid loaders, such as anion exchangers of the SLC4 and SLC26 gene families, whose activity reduces pHi.[4,26,27] Since anion exchangers contribute to steady-state pHi by balancing the activity of acid extruders,[18,28] we speculate that the alkalization observed in acid-adapted cancer cells arises from a suppression of acid loading. Anion exchangers (AEs) of the SLC4 family comprise the Na^+-independent Cl^-/HCO_3^- exchangers AE1, AE2, and AE3, which have well-documented roles in acid-base transport.[29] Whereas AE1 is primarily expressed in erythrocytes, AE2 and AE3 are widely distributed in epithelia, particularly in the kidney and gut.[26] Members of the SLC26 family include anion (Cl^-/HCO_3^-) exchangers, with high *SLC26A3* expression in the colon and duodenum.[27] Recent literature has implicated AE2 activity in leaking H^+ ions across the Golgi membrane, thereby alkalinizing the Golgi lumen.[30] This system can be very effective in re-distributing H^+ ions between the cytoplasm and the Golgi. Unless the contents are expunged, this pHi-regulatory strategy is not sustainable under continuous metabolic acid production. In contrast, AE2 activity at the surface membrane is strategically placed to oversee acid-base traffic between the cell and its environment. However, the role of surface-expressed AE2 in setting steady-state pHi of cancer cells is poorly understood.

Using a panel of 66 colorectal cancer (CRC) cell lines, covering various permutations of mutations, we characterized the steady-state relationship between pHi and pHe. We identified AE2 (*SLC4A2*) as a regulator of steady-state pHi. In acidic environments, surface-expressed AE2 undergoes lysosomal degradation that raises pHi back into the physiological range. This process is triggered by inhibition of the mTOR pathway and can be reversed with lysosomal inhibitors. As a mechanism conferring a survival advantage in acidic microenvironments, we propose inhibition of AE2 degradation as a strategy for cancer treatment.

RESULTS

Relationship between pHe and pHi in CO_2/HCO_3^- buffer across a panel of colorectal cancer cell lines

Mechanisms of acid adaptation could be inferred by screening a large panel of cell lines for pHi-regulatory phenotype and seeking those that are more capable of maintaining physiological pHi at low pHe. Using a high-throughput fluorescence imaging platform, we captured steady-state pHi at single-cell resolution over a range of pHe in a panel of 66 CRC cell lines (Figure S1).[31] Medium pH was adjusted by varying [HCO_3^-] under an atmosphere of 5% CO_2. Figures 1A and 1B show exemplar data from a cell line with a shallow (Colo678: +0.18) and with a steep (HDC9: +0.5) pHe-pHi slope.

We first tested the degree to which the pHe-pHi slope reflects the pHi-regulatory phenotype of CRC cells. Measured pHi was plotted against the pHe-pHi slope for all 66 lines, grouping data by pHe. This produced six regression lines, one per pHe level, with y-axis intercepts that were not significantly influenced by pHe (Figure 1C). Treating this intercept as a cell-line-independent constant, it is possible to predict a cell line's pHi at a given pHe using information about the slope. The most striking observation is that no cell line was able to maintain a physiological pHi (~7.2) in acidic medium (pHe <7). Restoring pHi into the physiological range under acid stress would require a transcriptional or post-translational adaptation. A second parameter describing a cell line's pHi-regulatory phenotype relates to cell-to-cell heterogeneity, which may reflect variation in the activity of transporters. Figures 1D and 1E show histograms of pHi in DLD1 or SNUC1 cells incubated at pHe 7.4 or 6.9. Wider distributions indicate greater heterogeneity of pHi control. Game theory, which can model carcinogenesis, argues that greater variation facilitates evolution.[32] Thus, cell lines manifesting greater cell-to-cell variation in pHi control may be more successful in evolving fitter phenotypes under acid selection. Using information about the pHe-pHi slope and pHi standard deviation, we grouped CRC lines by k-means clustering into "regulators" (shallow pHe-pHi slope), "trackers" (steep pHe-pHi slope), "tight controllers" (narrow pHi distribution), and "loose controllers" (wide pHi distribution) (Figure 1F). Slopes ranged from 0.18 to 0.5 (Figure 1G) and standard deviations spanned from 0.05 to 0.18 (Figure 1H). There was no correlation between slope and standard deviation ($R^2 = 0.00053$). Table 1 lists the CRC cell lines according to their pHi-regulatory phenotype.

Next, we tested whether the pHi-regulatory phenotype was hardwired. For this, we used fluorescence-activated cell sorting (FACS) to extract the 10% most alkaline and 10% most acidic HCT116 cells, using the cSNARF1 fluorescence ratio. Strikingly, the disparity in pHi of the sorted sub-populations was not maintained in subsequent culture (Figure S2). This indicates that differences in pHi-regulatory phenotype are unlikely to arise from clonal expansion of specific mutations or stable epigenetic differences, but rather stochastic variation linked to transient changes in gene expression, protein abundance, and/or activity. The reason acidic and alkaline sub-populations return to the parent heterogeneity may relate to underlying cyclic events that influence pHi, such as the cell cycle or metabolic rhythms.[33,34]

Figure 1. Relationship between pHe and pHi in CO_2/HCO_3^- buffer across a panel of colorectal cancer cell lines

(A and B) pHe-pHi relationship in (A) Colo678 cells and (B) HDC9 cells measured using cSNARF1 fluorescence, showing best-fit line. Mean of three independent repeats (triplicate technical repeats). Error bars represent standard deviation in the population.

(C) Relating steady-state pHi with slope across all cell lines, grouped by pHe. Multivariate regression indicates common y-axis intercept. pHi can be predicted from the pHe-pHi slope (a cellular variable) and pHe (an environment variable), with a cell line-independent y-axis intercept.

(D and E) Histograms of pHi (measured at pHe 7.4 and pHe 6.9) for (D) DLD1 and (E) SNUC1 cells.

(F) k-means clustering of cell lines according to their pHe-pHi slope and standard deviation of steady-state pHi (each data point represents a cell line).

(G and H) Ranking cell lines according to (G) slope of pHe-pHi relationship and (H) standard deviation of pHi.

Table 1. Lists of colorectal cancer cell lines according to pHi phenotype determined by k-means clustering shown in Figure 1F

Regulators	Trackers	Tight control	Loose control
CL40	C10	C32	C106
COLO205	CAR1	C99	C2BBE1
COLO206	COLO320HSR	CACO2	CCK81
COLO678	HCC56	CC20	CCO7
GP5D	HCT116	COLO320DM	HDC111
LS513	HDC9	CX1	HDC82
SW1417	HT29	DLD1	HRA19
SW403	HT55	GP2D	NCIH508
SW480	LOVO	HCC2998	NCIH548
	NCIH747	HCT15	OXCO2
	SKCO1	HDC114	RCM1
	SNUC2B	HDC54	RW7213
	SW837	HDC57	SNUC1
	T84	JHCOLOY1	SW1222
		LS174T	VACO4S
		LS180	
		LS411	
		OUMS23	
		PMFKO14	
		RKO	
		RW2982	
		SNU1235	
		SW48	
		SW620	
		SW948	
		VACO10MS	
		VACO4A	
		VACO5	

Correlating pHi-regulatory phenotype with gene expression

Correlating gene expression with phenotype in a large panel of cell lines is an unbiased approach for identifying novel genes linked to pHi regulation. To that end, we performed a statistical analysis of differentially expressed genes (DEGs) for "regulator" vs. "tracker" and "tight controller" vs. "loose controller" pairs.

Comparing regulator vs. tracker cell lines (Figure S3), we identified significantly higher expression of BCL2-interacting protein (*BNIP3*) and *PEG10* in the former, but neither is canonically linked to pHi regulation. Among genes linked to pHi, *SLC16A7* (MCT2) had higher mRNA levels in tracker cell lines. However, correlation does not imply causality, and small interfering RNA (siRNA) knockdown of these genes did not change the pHe-pHi slope (Figure S4A). Thus, these DEGs may have only an indirect link to pHi or represent compensatory mechanisms. We found higher expression of V-type ATPase isoform *ATP6V0A2* in regulator cells. Its knockdown increased the pHe-pHi slope, suggesting a mechanistic link to pHi (Figure S4B). Cell lines showing a wide distribution of pHi had higher expression of *CEACAM6*, but lower expression of *PMP22*. Among genes with established links to pHi, *CA9* was highly expressed in tight regulators. We validated these correlations using siRNA knockdowns. Inactivation of *CEACAM6* led to a narrower pHi distribution, an effect that may relate to changes in cell adhesion (Figure S4C; significant effect detected at pHe 7.4). In contrast, *CA9* knockdown widened the pHi distribution, which is consistent with the enzyme's role in facilitating CO_2/HCO_3^- diffusivity (Figure S4D; significant effect detected at pHe 6.4).

It was striking that some of the key genes deemed important for pHi regulation (e.g., *SLC9A1*, *SLC4A2, SLC4A7*) did not emerge in our gene expression-phenotype correlations (Figure S5). Moreover, gene ontologies related to pHi regulation or glycolytic acid production were not enriched in any of the CRC categories (Tables S1 and S2). Gene enrichment analysis did, however, indicate a tendency for tracker cells to be associated with genes belonging to certain metabolic pathways, such as regulatory systems. It is plausible that such pathways contribute to the tracker pHi-regulatory phenotype, because many metabolic processes are net producers of acid or base.

Finally, we performed Fisher's exact test to determine whether there was a correlation between pHi-regulatory phenotype and common driver mutations. We observed no significant correlation between *PIK3CA*, *p53*, *KRAS*, *BRAF*, *β-catenin*, or *APC* mutation status and readouts of pHi (Table S3). We therefore focused on post-transcriptional and post-translational mechanisms as candidates for acid adaptation of pHi control under acid stress.

Anion exchanger activity sets steady-state pHi

Resting pHi is ultimately set by surface-expressed proteins that transport H^+ equivalents. Yet, gene expression analyses found no compelling genetic correlation with pHi-regulatory phenotype. To further investigate the transporters responsible for setting resting pHi, we interrogated the mechanisms functionally using ion substitutions and inhibitor drugs. We inhibited the key acid extruder NHE1 (*SLC9A1*) with cariporide under a CO_2/HCO_3^--buffering regime (Figures 2A and S6). However, only a small decrease in pHi was observed in three tracker (HDC9, LOVO, HT55) and two regulator cell lines (Colo206, Colo678). While NHE1 is required for extruding bouts of intracellular acidity, it appears to be less important for fine-tuning steady-state pHi in CRC lines.

HCO_3^--dependent acid extruders have been linked to pHi control. If these played a critical role in setting resting pHi, then removal of their substrate is expected to acidify cells. Substrate (HCO_3^-) was removed at constant pHe by replacing CO_2/HCO_3^- buffer with HEPES/MES. Strikingly, this intervention alkalinized both tracker and regulator cell lines (Figures 2B and S6). This observation indicated that the net direction of HCO_3^--dependent transport is acid loading. Such a flux could be carried by members of the SLC4 and SLC26 family of AEs.

To confirm the involvement of Cl^-/HCO_3^- exchangers, we performed measurements in CO_2/HCO_3^--buffered medium that had reduced levels of Cl^-, iso-osmotically replaced with gluconate salts. Removal of Cl^- raised the steady-state pHi, consistent with a reduction in the acid loading by AEs (Figures 2C and S6). The response was more prominent in cell lines with steeper pHe-pHi slopes (HDC9, LOVO, and HT55), whereas in lines of

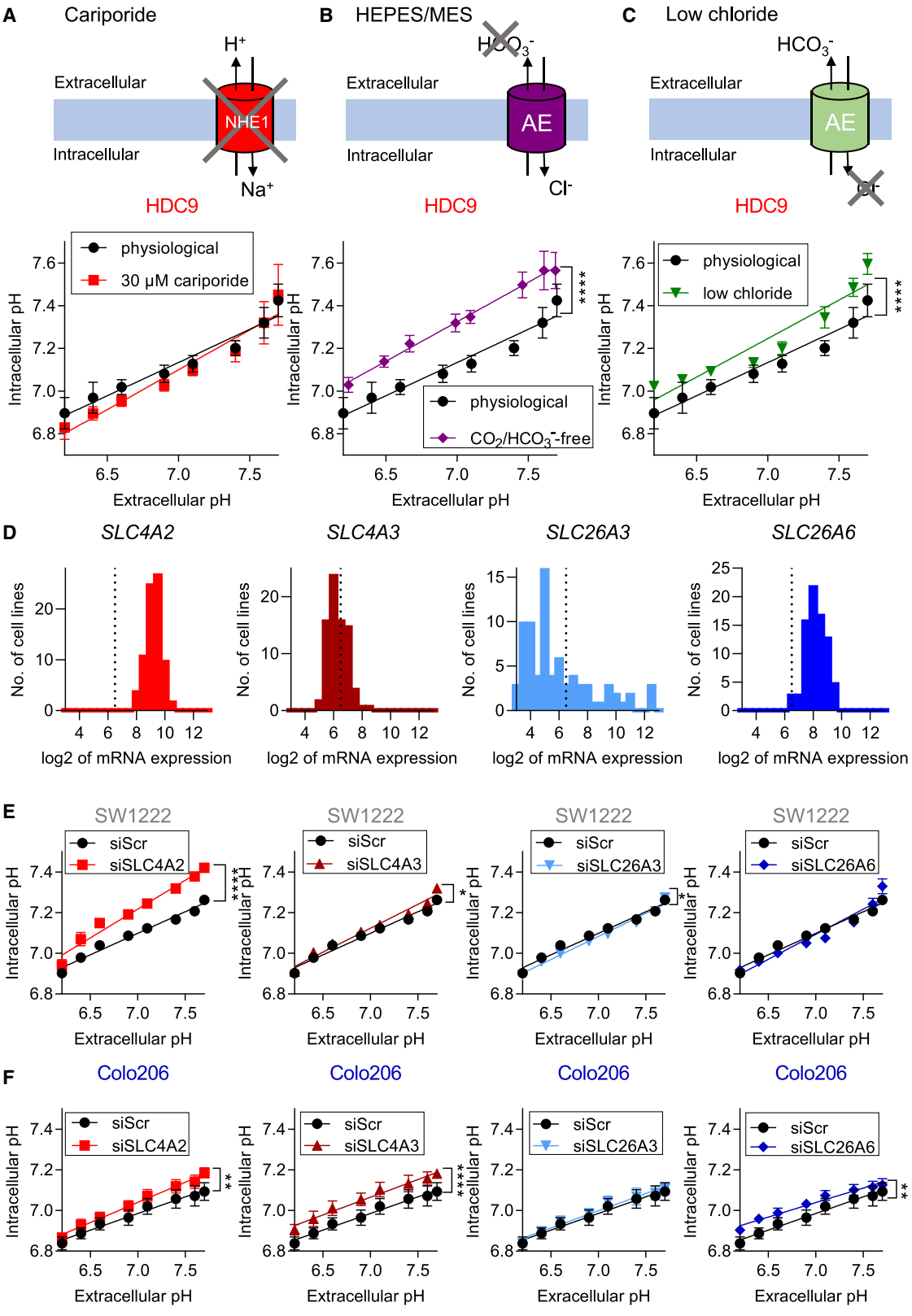

(legend on next page)

shallow slope (Colo678 and Colo206), it was apparent in the acidic range of pHe. Taken together, the results implicate a role for AEs in setting resting pHi. A plausible mechanism of alkalization in acid-adapted cells may involve AE inhibition or downregulation.

We sought to identify the AEs responsible for setting pHi. Based on mRNA levels, *SLC4A2*, *SLCA3*, *SLC26A3*, and *SLC26A6* are candidates for such transporters in CRC lines (Figure 2D). Whereas *SLC4A2* and *SLC26A6* are expressed in all cell lines, *SLC4A3* and *SLC26A3* expression was above background in only a subset of cell lines (Figure 2D). Moreover, Gaussian mixture modeling suggested a bimodal pattern of *SLC26A3* gene expression, suggesting a link with inactivating mutations or stable epigenetic changes.[35] We tested the effects of siRNA-mediated knockdown of these transporters in seven cell lines representative of shallow (Colo678, Colo206), intermediate (C99, SW1222, DLD1), or steep pHe-pHi slope (HDC9, HT55) (Figure S7). *SLC4A2* knockdown raised the pHi in Colo678, Colo206, C99, SW1222, and DLD1 cells (Figures 2E, 2F, and S7). *SLC4A2* knockdown had a weak or no effect on pHi in cells with a steep pHe-pHi slope (e.g., HDC9 and HT55; Figure S7). These cell lines nonetheless express AE2 and demonstrate high siSLC4A2 knockdown efficiency (Figure S8). Loss of *SLC4A3* in Colo206 cells led to a comparable pHi shift as with *SLC4A2* knockdown (Figure 2F). However, *SLC4A3* is expressed only in a subset of the cell lines and is unlikely to be a general mechanism (Figure S8). Knockdown of *SLC26A3* and *SLC26A6* had a considerably smaller effect on pHi in all cell lines tested (Figures 2E, 2F, and S7).

To summarize, our results argue that pHi control in tracker cell lines (i.e., steep pHe-pHi slope) is relatively unresponsive to genetic inactivation of AE2. At physiological pHe, the cytoplasm of these lines is already alkaline, indicating that AE2 is not contributing significant acid-loading flux toward lowering pHi. *SLC4A2* knockdown in these cells does not affect pHi phenotype. In contrast, regulator cell lines have a lower pHi at physiological pHe, which indicates a larger acid-loading flux carried by AE2. Here, *SLC4A2* inactivation is expected to raise pHi.

Intracellular alkalization in acid-adapted cells arises from loss of AE2 activity

Analysis of pHe-pHi relationships (Figure 1C) reveals that a reduction in pHe inadvertently reduces pHi. However, this response was measured within tens of minutes, which precludes any longer-term adaptive mechanisms. To identify slower-onset adaptive responses that may influence pHi homeostasis, we cultured cells under acidic (pHe 6.4) conditions for 1 week and thereafter measured pHi over a range of pHe varied acutely (Figure 3A). Control experiments used cells that had been kept at pH 7.4 for 1 week. Prolonged exposure to acidic medium led to a robust rise in pHi in cell lines with steep (HT55; Figure S9) and intermediate slope (SW1222, DLD1; Figures 3B and S9). In HT55 cells, the acid-adaptation response of pHi was uniform across the pHe range, whereas in SW1222 and DLD1, it tended to be more prominent over the alkaline pHe range.

Next, we tested the reversibility of these adaptive responses. A second series of experiments included a 1-week recovery period in pH 7.4 for both control and acid-adapted cells. In all cell lines tested, we observed indistinguishable pHe-pHi relationships in the two groups on day 14 (Figures 3C and S9). These findings confirm that the alkaline shift in acid-adapted cells is reversible and, therefore, unlikely to arise from permanent changes, such as selection, although irreversible changes may arise when cancer cells are grown in acidic medium for considerably longer periods. Instead, we speculate that acid adaptation of pHi is evoked by a transcriptional response or altered protein function. We also observed an alkaline shift in pHi in acid-adapted pancreatic ductal adenocarcinoma (PDAC) cell lines, suggesting a more general phenomenon (Figure S9).

The effect that acid adaptation has on pHi resembles that of *SLC4A2* knockdown. Therefore, we speculated a role for reduced AE2 function in the acid-adaptation mechanism. In all cell lines tested, exposure to acidic medium for 1 week strongly reduced AE2 protein levels (Figures 3D and S10). In two cell lines (COLO678, DLD1), a lower-molecular-weight AE2 band was visible after acid adaptation, possibly indicating protein degradation. The reduction in AE2 protein level was not due to a reduction in *SLC4A2* mRNA, as determined by qRT-PCR (Figure S10). This may explain why *SLC4A2* was not detected as differentially expressed between CRC cell line categories. Long-term exposure to low pHe reduced AE3 protein levels in a subset of cell lines (Colo206, C99), but raised levels in others (HT55, Colo678; Figures 3D and S10). We observed strong induction of SLC26A3 in HT55 cells upon treatment with acidic medium. Acid adaptation did not evoke a consistent change in expression of the protein product of *SLC26A6* (Figure S10).

Next, we tested whether the reduction in AE2 protein was triggered by a fall in pHi secondary to medium acidification or was a direct effect of low pHe. We observed a reduction in AE2 in cells with genetically inactivated respiration (SW1222 *NDUFS1*$^{-/-}$), which forces a compensatory increase in glycolysis that acidifies the cytoplasm. The loss of AE2 protein is likely a direct response

Figure 2. Anion exchanger activity sets steady-state pHi

(A) pHe-pHi relationship in HDC9 cells under physiological buffering (CO_2/HCO_3^-) in the presence or absence of 30 μM cariporide (NHE1 inhibitor). Error bars represent standard deviation.

(B) pHe-pHi relationship in HDC9 cells measured in physiological buffering or CO_2/HCO_3^--free buffer (HEPES/MES).

(C) pHe-pHi relationship in HDC9 cells in CO_2/HCO_3^- buffer containing normal or reduced [Cl^-] (replaced with gluconate salts). Mean ± SEM of three biological repeats (triplicate technical repeats).

(D) mRNA levels for *SLC4A2*, *SLC4A3*, *SLC26A3*, and *SLC26A6* in a panel of 120 CRC cell lines. Black dotted line represents background levels of gene expression, separating "low" and "high" expressing lines.

(E and F) pHe-pHi relationships measured under physiological buffering conditions in (E) SW1222 cells or (F) Colo678 cells treated with siRNAs for *SLC4A2*, *SLC4A3*, *SLC26A3*, or *SLC26A6*. Mean ± SEM of three biological repeats (triplicate technical repeats). Significance testing by two-way ANOVA and Tukey's test for multiple comparisons (*p < 0.05, **p < 0.01, ****p < 0.0001; ns, non-significant). Error bars represent standard deviation.

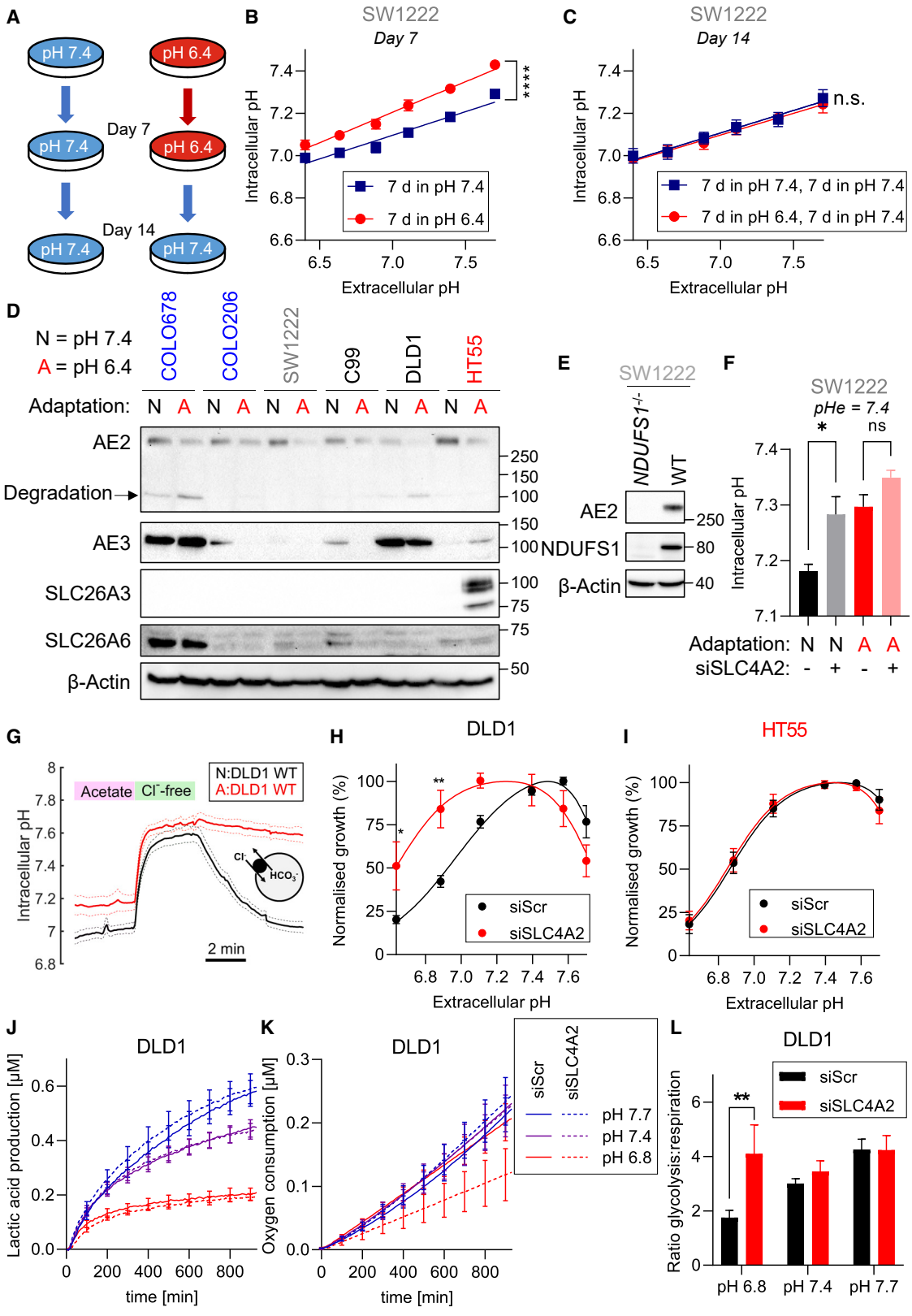

(legend on next page)

to low pHi, rather than low pHe (Figures 3D and S10). To verify that the alkalization of acid-adapted cells was due to AE2 loss, we transfected acid-adapted and control cells with siSLC4A2. *SLC4A2* knockdown led to a significant increase in pHi in control cells, but not in acid-adapted cells (Figure 3F).

AE2 is present in various subcellular compartments, including the surface membrane and organelles. Previous studies have implicated a role for AE2 in maintaining the structural integrity of the Golgi apparatus,[36] where it also contributes to regulating intraluminal pH.[30] However, the abundance of AE2 in this organelle is cell-type specific.[37] To test for AE2 compartmentalization, we performed immunofluorescence on DLD1 and SW1222 cells. We found a widespread distribution in both cell lines (Figure S11). Specifically, AE2 co-localized with the membrane marker EPCAM and, to a lesser degree, the Golgi marker GM130. In DLD1 cells, 25% of the AE2 signal was associated with EPCAM and only 5% with GM130; these numbers for SW1222 are 20% and 9%.

We sought functional evidence for AE2 activity at the surface membrane by measuring Cl^-/HCO_3^- exchange flux and its response to acid adaptation. Flux was tracked by live-cell fluorescence imaging of pHi (Figure 3G). A series of solution maneuvers controlled the thermodynamic driving force that applies to surface-expressed AE protein only. DLD1 cells, under superfusion with CO_2/HCO_3^--buffered solutions, were acid loaded by means of an acetate pre-pulse. Switching the superfusate to acetate-free, chloride-free solution caused a rebound alkalinization of cells. The absence of Cl^- inactivates any AE proteins present. Upon re-introduction of Cl^--containing solution, the combination of an inward Cl^- gradient and raised pHi is a strong driving force for Cl^-/HCO_3^- exchange by AE, if the proteins are expressed at the surface membrane. In wild-type DLD1 cells that had been adapted to physiological pHe, Cl^- re-addition evoked an immediate and fast acid-loading response, which can be explained only in terms of surface-expressed AE. To quantify AE activity, we calculated H^+-equivalent flux as the product of pHi change and buffering capacity (Figure S13D). The Cl^--activated acid influx was reduced by 66% in *SLC4A2*-knockout (KO) DLD1 cells (Figure S13C), indicating that two-thirds of AE activity in wild-type DLD1 cells can be attributed to AE2. In wild-type DLD1 cells that had been adapted to low pHe, Cl^--activated acid influx was reduced ~90%. Thus, acid adaptation of wild-type DLD1 cells arises from the loss of surface-expressed AE2 activity and protein.

Genetic inactivation of *SLC4A2* leads to reduced acid sensitivity of growth and metabolic changes

We investigated whether the rise in pHi, triggered by AE2 loss, has consequences for cell survival and metabolism. In DLD1 and SW1222 cells, *SLC4A2* knockdown shifted the pHe sensitivity of cellular growth to a more acid-resistant phenotype (Figures 3H and S9H). In contrast, *SLC4A2* knockdown in HT55 cells did not change the pHe dependence of growth, consistent with the lack of effect on pHi in these cells (Figure 3I). These results indicate that AE2 activity influences growth through changes in pHi. Loss of AE2 function could underpin a survival mechanism under acid stress.

Given that cytoplasmic pH modulates glycolytic enzymes,[6,38] raising the pHi by *SLC4A2* knockdown is expected to make glycolysis less pH sensitive. To test this, we used a fluorimetric assay of pHe and dissolved O_2 to measure glycolytic and respiratory rates. In cells with normal *SLC4A2* expression, a reduction in pHe strongly inhibited glycolysis (Figure 3J) without affecting respiration (Figure 3K). Low pHe thus reduces the ratio of "carbon" flux through glycolysis relative to respiration (Figure 3L). While *SLC4A2* knockdown did not affect acid production at low pHe, it notably decreased O_2 consumption. Consequently, the ratio of carbon flux through glycolysis relative to respiration became pHe insensitive. We infer that the loss of AE2 in acid adaptation allows glycolysis to make a greater contribution to overall energetics. Consequently, relative flows through glycolysis and respiration remain largely pHe insensitive in

Figure 3. Intracellular alkalization in acid-adapted cells arises from loss of AE2 activity

(A) Experimental workflow for acid adaptation and recovery. Cells were cultured in CO_2/HCO_3^--buffered medium supplemented with 10 mM MES (to augment buffering) at either pH 7.4 or pH 6.4 for 7 days. Culture was extended for another 7 days in medium at pH 7.4 to investigate reversibility.

(B and C) pHe-pHi relationship in SW1222 cells measured (B) after acid adaption (day 7) and (C) after recovery (day 14). Mean of four biological repeats, each carried out in triplicate. ****$p < 0.0001$. Error bars represent standard deviation.

(D) Western blot showing protein products of *SLC4A2* (AE2), *SLC4A3* (AE3), *SLC26A3*, and *SLC26A6* in acid-adapted or control cells.

(E) Western blot showing AE2 and NDUFS1 levels in SW1222 wild-type (WT) and *NDUFS1*$^{-/-}$ cells.

(F) Acid-adapted or control SW1222 cells were transfected with non-targeting siRNA or siSLC4A2 for 72 h prior to pHi measurements at pHe 7.4. Data shown are mean ± SEM of three biological repeats, carried out in triplicate; *$p < 0.05$.

(G) Protocol for interrogating AE-dependent acid-loading flux, a functional assay of AE proteins at the surface membrane. Wild-type DLD1 cells were adapted to either pH 7.4 or pH 6.4 for 72 h prior to measurements and plated in superfusion chambers. Cells were loaded with cSNARF1 to image pHi and superfused with a sequence of solutions to measure chloride-evoked AE activity. The protocol consisted of 8 min in 80 mM acetate-containing solution, followed by 3 min in acetate-free, chloride-free solution and then in solution containing normal [Cl^-]. All superfusates were CO_2/HCO_3^- buffered at pH 7.4. Data shown are mean ± SEM of four biological repeats; the mean represents the average of 150–250 cells.

(H and I) Normalized growth (sulforhodamine B [SRB] absorbance) at 6 days as a function of pHe in siSLC4A2-treated (H) DLD1 cells or scrambled controls and (I) in HT55 cells (normalized to growth at optimum pHe). Mean ± SEM of three to six independent repeats (triplicate technical replicates). Significance determined with two-way ANOVA using Sidak's multiple comparisons test (*$p < 0.05$, **$p < 0.01$; ns, non-significant). Error bars represent SEM.

(J and K) Paired time courses of (J) acid production and (K) O_2 consumption at different starting pHe in DLD1 cells. pHe and O_2 were measured using 8-hydroxypyrene-1,3,6-trisulfonic acid trisodium salt (HPTS) and tris(bipyridine)ruthenium (II) chloride (RuBPY) fluorescence, respectively, in medium buffered with 0.5% CO_2 and 8 mM HCO_3^-. Cells were treated with siRNAs for Scramble (solid lines) or *SLC4A2* (dashed lines) 72 h prior to measurements. Error bars represent SEM.

(L) Ratio of cumulative glycolytic to respiratory activity (expressed in terms of glucose metabolism) over the studied range of pH in *SLC4A2* knockdown and scrambled control DLD1 cells. Calculated assuming lactic acid/glucose stoichiometry of 2 and O_2/glucose stoichiometry of 6. Mean of six independent repeats, carried out in five technical repeats. Significance determined with two-way ANOVA using Sidak's multiple comparisons test (**$p < 0.01$; ns, non-significant).

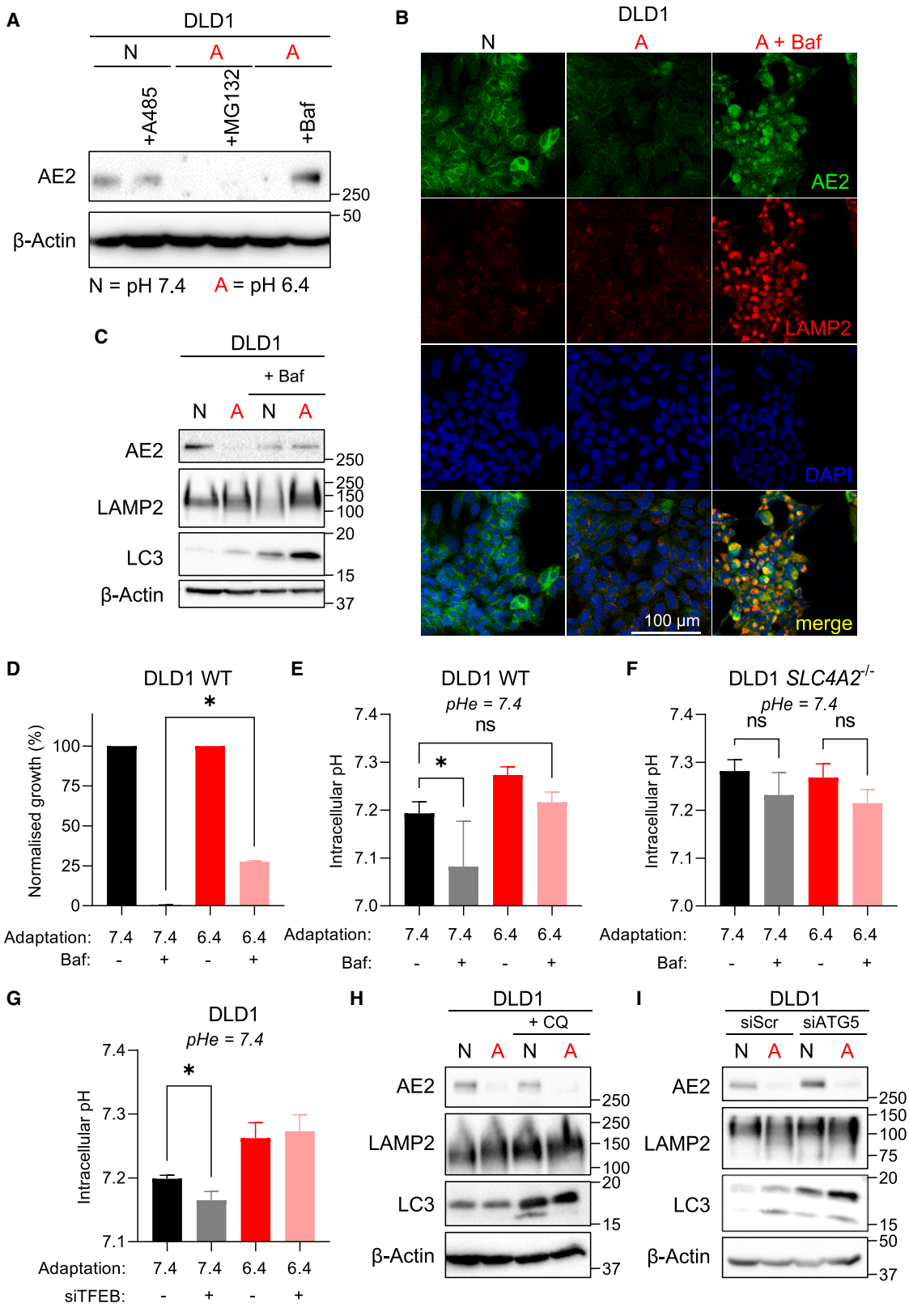

(legend on next page)

SLC4A2-deficient cells, whereas control cells must redirect flux toward respiration at low pHe.

Blocking lysosomal function reverses AE2 degradation

To further investigate the mechanism of AE2 downregulation, we used DLD1 cells, which belong to the tight control pHi-regulatory phenotype and have excellent dye-retention properties. There are a myriad of potential links between low pHe and AE2 degradation. Low pHe has been shown to reduce histone acetylation.[39] However, reducing histone acetylation pharmacologically using the p300/CBP inhibitor A485 did not meaningfully affect AE2 levels (Figures 4A and S12). Since *SLC4A2* mRNA levels did not respond significantly to acid adaptation, an alternative mechanism explaining the loss of AE2 function is protein degradation. Treating cells with the protein synthesis inhibitor cycloheximide decreased AE2 levels over time, regardless of whether the cells had been adapted to medium at physiological or low pHe (Figure S12). We therefore conclude that AE2 protein undergoes considerable turnover, but its *de novo* synthesis ensures higher surface expression at physiological pHe.

Acid adaptation in the presence of the proteasome inhibitor MG132 did not rescue AE2 levels in acid-adapted cells (Figures 4A and S12). Immunoprecipitation of endogenous AE2, followed by probing with an anti-ubiquitin antibody, showed that AE2 is not ubiquitinated. These results provide further evidence against proteasomal degradation as a mechanism for regulating AE2 levels (Figure S12). In contrast, blocking lysosomal function using bafilomycin A1 rescued AE2 protein levels in acid-adapted cells (Figures 4A and S12). Immunofluorescence staining for AE2 and the lysosomal marker LAMP2 revealed low AE2 abundance in acid-adapted cells, but levels were restored when bafilomycin A1 was added during acid adaptation (Figure 4B). Furthermore, bafilomycin A1-treated cells had raised LAMP2 levels co-localizing with AE2. Consistent with previous reports linking acidosis and lysosomal function,[20] acid-adapted cells showed a modest increase in LAMP2 expression and the autophagy marker LC3[40] (Figures 4C and S12). LC3 and LAMP2 levels increased further with bafilomycin A1 treatment, indicating that bioavailability of the drug had not been compromised at low pHe. Strikingly, cells cultured in medium at physiological pHe are exquisitely sensitive to bafilomycin A1, to the extent that 72 h of treatment at 10 nM invariably led to cell death (Figure 4D). As a result, AE2 expression and pHi (Figures 4C and 4E) had to be recorded in a small population of surviving cells, which may cause AE2 levels to be underestimated. In striking contrast, acid-adapted cells were able to survive bafilomycin A1 treatment, although cell growth was reduced compared with untreated cells.

We next tested whether the changes in AE2 levels evoked by bafilomycin A1 also affected pHi. In wild-type DLD1 cells cultured under physiological pHe, bafilomycin A1 reduced pHi (Figure 4E). The magnitude of this effect may be underestimated, as the analysis excluded dying cells that may have succumbed to acidosis. In acid-adapted cells, bafilomycin A1 reversed the effect of acid adaptation and reduced pHi back to "non-adapted" levels. Conversely, in DLD1 cells with *SLC4A2* genetically inactivated using CRISPR-Cas9 (Figure S13), bafilomycin A1 did not significantly affect the pHi in acid-adapted or non-adapted cells (Figure 4F).

Taken together, our data show that long-term exposure to acidic conditions leads to a degradation of AE2 protein by lysosomes and that inhibiting lysosomal function with bafilomycin A1 can rescue AE2 protein levels. Furthermore, cytoplasmic acidification evoked by bafilomycin A1 is, at least partly, mediated through AE2 activity.

We sought to confirm the link between lysosomal function and pHi through genetic inhibition of *TFEB*, a transcription factor responsible for lysosomal biogenesis.[41] Similar to the effects of bafilomycin A1 on pHi, siRNA-mediated *TFEB* knockdown decreased the pHi of cells cultured under physiological pHe but not in acid-adapted cells (Figure 4G). We also explored other means of inhibiting lysosomal function, such as treatment with glycyl-L-phenylalanine 2-naphthylamide (GPN), to disrupt lysosomal integrity, or the autophagy inhibitor chloroquine (CQ). Treatment with GPN or CQ did not rescue AE2 protein levels in acid-adapted cells (Figures 4H, S13, and S14). The ineffectiveness of CQ may relate to its weakly basic chemistry, which leads to reduced bioavailability at low pHe. This is evident from the reduction in LC3 signal (Figure 4H) and resistance to CQ toxicity at acidic pHe (Figure S13). Furthermore, CQ mainly inhibits autophagosome fusion with lysosomes, rather than affecting the degradative activity of lysosomes.[42] We therefore tested whether autophagy is involved in AE2 degradation by genetic ablation of *ATG5*, which codes for a protein involved in the formation of autophagic vesicles. However, *ATG5* knockdown did not affect AE2 protein levels in acid-adapted cells (Figures 4I and S14). Given

Figure 4. Blocking lysosomal function reverses AE2 degradation

(A) Western blot showing AE2 protein levels in DLD1 cells adapted to pH 7.4 for 72 h and treated with 5 μM A-485 (p300 inhibitor). Acid-adapted cells were treated with 50 nM MG132 or 10 nM bafilomycin A1.

(B) Immunofluorescence staining for AE2 (green) and LAMP2 (red) in DLD1 cells adapted to pH 6.4 for 72 h, with or without bafilomycin A1 treatment (10 nM). Images are representative of three independent repeats.

(C) Western blot showing AE2, LAMP2, and LC3 protein levels in acid-adapted or control cells, with or without 10 nM bafilomycin A1 treatment (72 h).

(D) Normalized growth (SRB absorbance) in acid-adapted or control cells, with or without treatment with 10 nM bafilomycin A1 (72 h). Data are plotted as relative cell growth normalized to untreated controls (mean ± SEM of four independent repeats, three technical replicates).

(E and F) pHi in DLD1 (D) WT or (F) *SLC4A2*$^{-/-}$ cells adapted to either pH 7.4 or pH 6.4 for 72 h. Cells were either untreated or treated with 10 nM bafilomycin A1 for 72 h (mean ± SEM of four to six independent repeats, three technical replicates).

(G) pHi in DLD1 WT cells adapted to either pH 7.4 or pH 6.4 for 72 h. Cells were treated with siRNAs for Scramble or *TFEB* 72 h prior to measurements (mean of three independent repeats, three technical replicates). Significance determined with two-way ANOVA using Tukey's multiple comparisons test (*$p < 0.05$; ns, non-significant).

(H and I) Western blots showing AE2, LAMP2, and LC3 protein in cells adapted to pH 7.4 or pH 6.4, untreated or treated with (H) 25 μM chloroquine for 72 h or (I) siRNA for ATG5.

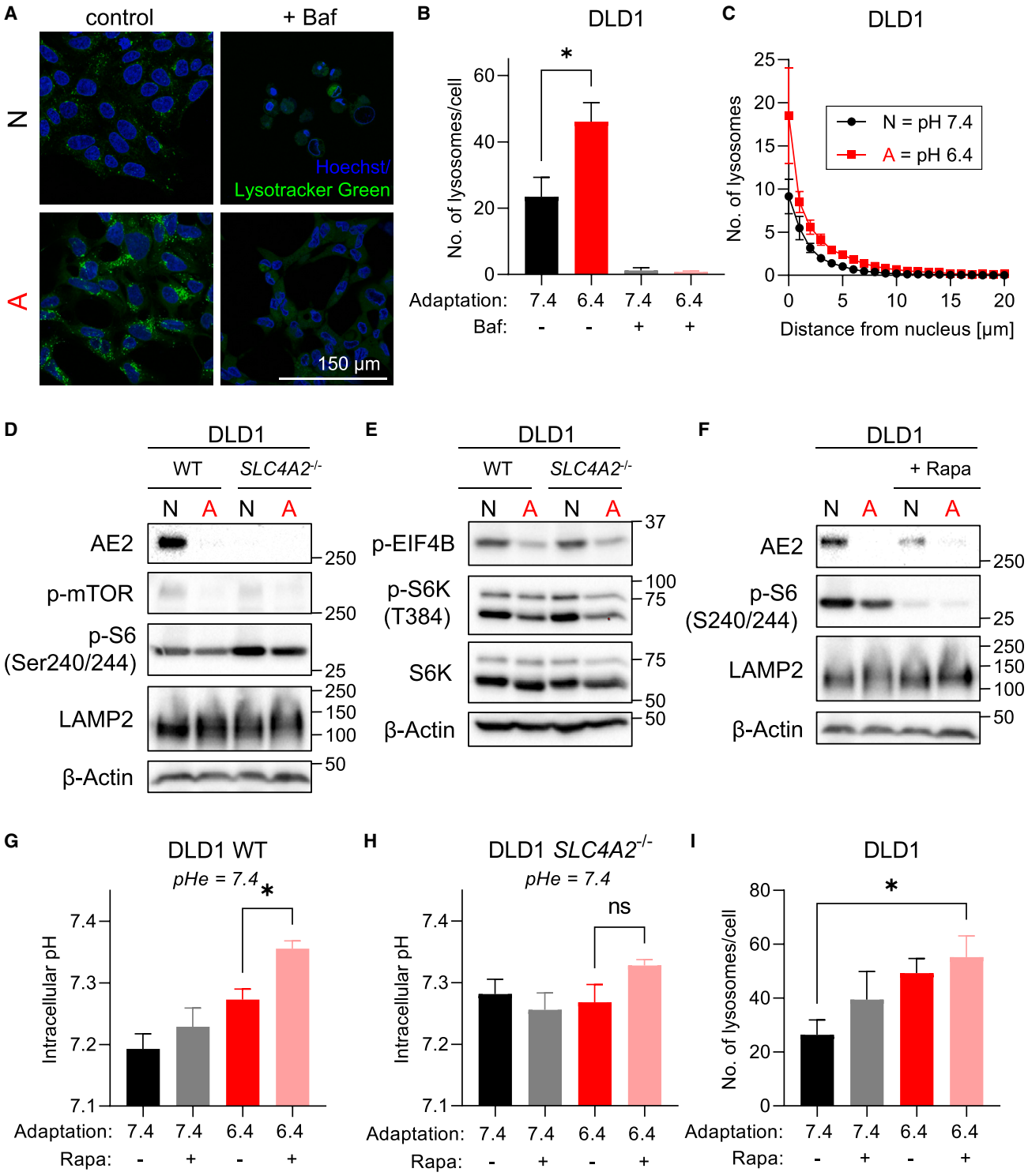

Figure 5. mTORC1 inhibition increases lysosomal function and AE2 degradation

(A) Images of lysosomes (LysoTracker Green DND-26) in acid-adapted or control cells treated for 72 h prior to imaging. Measurements were recorded in HEPES-buffered medium (pH 7.4).

(B) Quantification of data. Mean ± SEM of four independent repeats. Significance determined using paired t test (*p < 0.05).

(C) Radial distribution of lysosomes (relative to Hoechst-stained nucleus) in acid-adapted or control cells (mean ± SEM of four independent repeats).

(D and E) Western blots for AE2 and markers of mTOR pathway activity in DLD1 WT and DLD1 *SLC4A2*$^{-/-}$ cells adapted to pH 7.4 or pH 6.4.

(legend continued on next page)

the localization of AE2 at the surface membrane, degradation is likely to occur through endosomal internalization, rather than autophagy. Our results indicate that AE2 degradation is dependent on lysosomal acidity but unresponsive to autophagy inhibition.

mTORC1 inhibition increases lysosomal function and AE2 degradation

Given the link between AE2 expression and lysosomal function, we sought to identify the mechanisms triggering AE2 degradation. Acid-adapted cells had more lysosomes (LysoTracker fluorescence), compared with cells cultured Funder physiological pHe (Figures 5A and 5B). As expected, bafilomycin A1 abrogated LysoTracker fluorescence. Previous reports[20,43] observed a peripheral redistribution of lysosomes in response to acidity. However, in DLD1 cells, the radial distribution of lysosomal signal (expressed as distance from the nucleus) was only mildly affected by acid adaptation (Figure 5C). These results indicate that acid adaptation stimulates ensemble lysosomal activity, promoting acid-mediated AE2 degradation.

Previous studies have linked acid-evoked signaling to lysosomes through the inhibition of mTOR signaling.[43] Consistent with these reports, we found a reduction in several markers of mTOR pathway activity in acid-adapted cells (Figures 5D, 5E, and S15). Strikingly, we observed an increase in phospho-S6 (Ser240/244) in DLD1 *SLC4A2*$^{-/-}$ cells, which likely related to their more alkaline cytoplasm and the role of mTORC1 as a pHi sensor.[44] Recent studies have shown that mTORC1 activity controls the protein product levels of *SLC4A7*, a bicarbonate transporter of the same gene family as AE2.[45] Given the link between AE2 and lysosomal function, we tested whether pharmacological mTORC1 inhibition (rapamycin) also affects AE2 levels. To confirm efficacy, rapamycin reduced S6 phosphorylation (Figures 5F and S15). Rapamycin treatment decreased AE2 levels (Figures 5F and S15), akin to the effect of acid adaptation. While rapamycin had only a minor effect on pHi in DLD1 WT cells cultured under physiological pHe, a larger increase in pHi was observed in acid-adapted cells (Figure 5G). This could be explained by an additive effect of acid adaptation and rapamycin treatment on AE2 degradation. Conversely, rapamycin did not significantly change pHi in *SLC4A2*$^{-/-}$ cells, implicating AE2 as part of the response mechanism (Figure 5H). The combination of rapamycin treatment and acid adaptation led to a strong increase in the number of lysosomes, compared with control conditions (Figure 5I).

Acidity-triggered AE2 degradation occurs *in vivo*

We next sought to investigate AE2 expression in CRC patient samples (Figure 6A). In tumors matched with adjacent normal tissues, we observed a tendency for higher AE2 levels in normal tissue (Figures 6B, 6C, and S16). In contrast, LAMP2 levels were higher in most tumor tissues, compared with normal tissues (Figure 6C), which is in line with LAMP2 being a marker of acid adaptation.[20] Overall, we found a decrease in AE2/LAMP2 ratio in six of seven patient samples. We also investigated LAMP2 and AE2 expression in mouse xenograft tumors obtained from SW1222 and COLO320HSR tumors (Figure 6D). Strikingly, LAMP2 and AE2 signals occurred in distinct regions of the tumor, with very little overlap (Figures 6D and 6E). This indicates that high AE2 protein levels occur in alkaline tumor regions, whereas acid-adapted regions (marked by high LAMP2 levels) express less AE2 protein. These data demonstrate that AE2 degradation triggered by tumor acidity also occurs *in vivo*. In a clinical setting, high LAMP2 and low AE2 levels could be considered a biomarker for highly acidic tumors for use in disease diagnosis, targeted therapies, or guided surgery.

DISCUSSION

Here, we show that CRC cells adapt to acidic environments through lysosomal degradation of surface-expressed AE2, assayed functionally and by immunofluorescence. This process eliminates a widely expressed acid-loading transporter from the surface membrane, causing steady-state pHi to rise. In cancer cells adapted to acidic tumor microenvironments, this mechanism restores a physiological pHi that is conducive for progression and metastasis. We propose that acid-triggered AE2 degradation is a more general mechanism in cancer, as we also observed it in PDAC cells. The finding that cancer cells raise pHi by inactivating an acid-loading process represents a paradigm shift. Most prior research focused on the role of acid extruders, such as NHE1 or NBCn1.[1,46,47] Activating acid extrusion and reducing acid loading have equivalent effects on pHi, but the former raises ATP demand.

The mechanism that maintains an alkaline cytoplasm in an acidic environment was first investigated by screening a large panel of CRC cells for pHi-regulatory phenotype. The aim was to relate high pHi in a subset of CRC lines with DEGs that could arise from mutations or stable epigenetic changes. A screen of 66 CRCs revealed that no cell line was able to maintain a physiological pHi (7.2) when pHe was reduced below 7.0, at least on an acute timescale. By classifying cell lines according to pHi-regulatory phenotype, we identified gene correlations. These included the carcinoembryonic antigen 6 (*CEACAM6*), considered a promising avenue for cancer therapy,[48] and carbonic anhydrase 9 (*CA9*), a biomarker for tumor hypoxia.[49] Since the inactivation of correlating genes had only minor consequences for pHi homeostasis, we concluded that the mechanism for maintaining alkaline cytoplasm at low pHe was not linked to transcription.

By studying the processes that set resting pHi, we found that AE2 inactivation produced a robust rise in pHi, similar to

(F) Western blot for AE2, phospho-S6 (Ser240/244), and LAMP2 in DLD1 cells adapted to pH 7.4 or pH 6.4 for 72 h. Cells were either untreated or treated with 50 ng/mL rapamycin.
(G and H) pHi in DLD1 (G) WT and (H) *SLC4A2*$^{-/-}$ cells adapted to pH 7.4 or pH 6.4 for 72 h. Cells were either untreated or treated with 50 ng/mL rapamycin (mean ± SEM of six independent repeats). Significance determined with two-way ANOVA using Tukey's multiple comparisons test (*$p < 0.05$; ns, non-significant).
(I) Number of lysosomes per cell in DLD1 cells adapted to pH 7.4 or pH 6.4 for 72 h. Cells were either untreated or treated with 50 ng/mL rapamycin (mean ± SEM of four independent repeats, *$p < 0.05$).

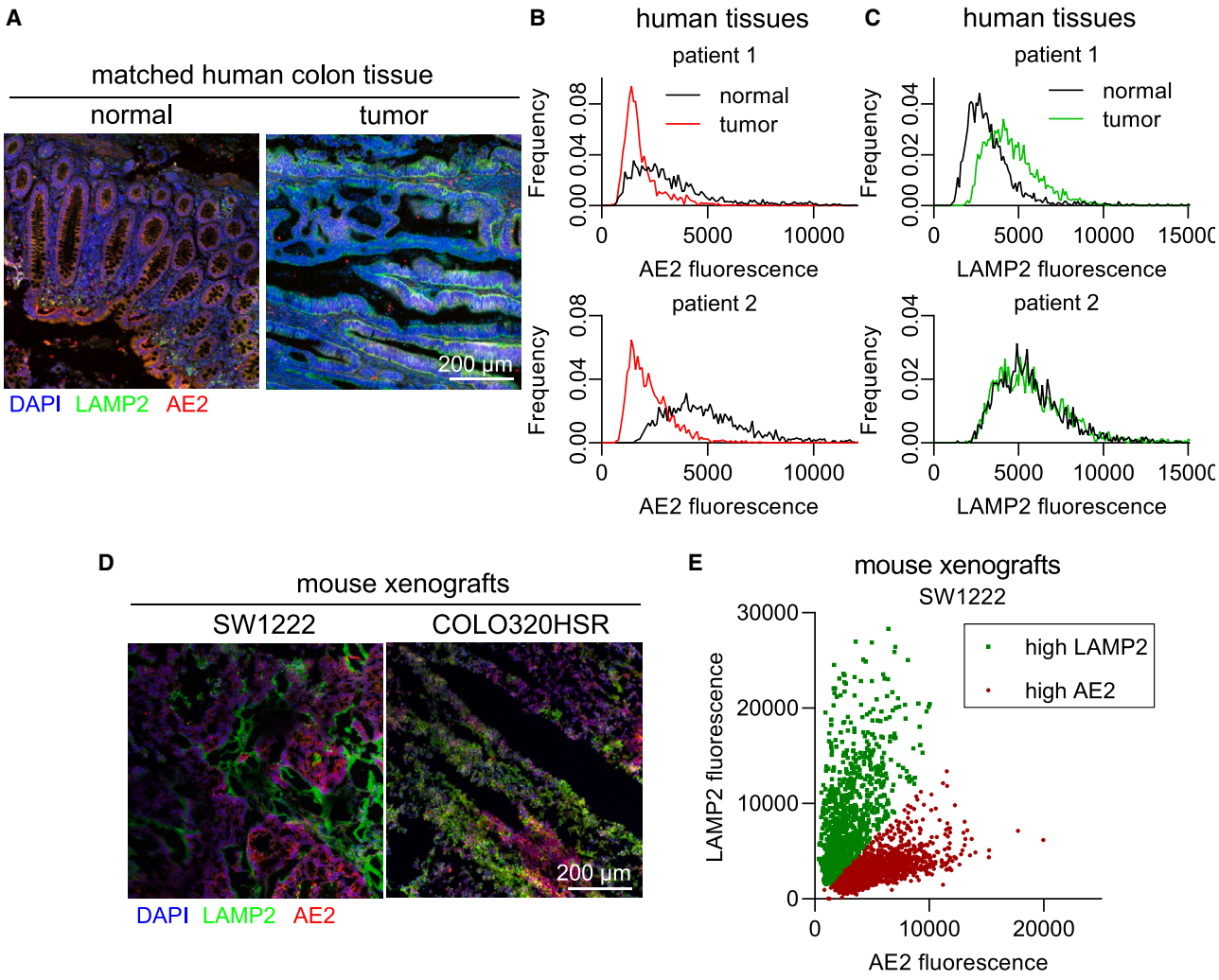

Figure 6. Acidity-triggered AE2 degradation occurs *in vivo*

(A) Representative images of AE2 (red), LAMP2 (green), and DAPI (blue) fluorescence in matched pairs of human normal colon and tumor formalin-fixed and paraffin-embedded (FFPE) tissue sections from colorectal cancer patients.

(B and C) Histograms of (B) AE2 and (C) LAMP2 fluorescence intensity per cell in matched pairs of human colon tumor tissues. Data shown for two individual patients.

(D) Representative images of AE2 (red), LAMP2 (green), and DAPI (blue) fluorescence in fresh-frozen tumor sections obtained from SW1222 and COLO320DM mouse xenografts.

(E) AE2 vs. LAMP2 fluorescence intensity per cell in SW1222 xenografts. Each dot represents one individual cell. Data shown are representative of xenografts from four animals.

that evoked by acid adaption. While AE2 degradation upon acid treatment was a general phenomenon, genetic inactivation of *SLC4A2* raised pHi in only a subset of cell lines. Notably, cell lines with a steep pHe-pHi slope (trackers) did not respond to *SLC4A2* knockdown, ostensibly because they are characterized by a high pHi. Thus, any further loss of AE2 activity would not have a meaningful effect on pHi. Using western blotting and immunofluorescence assays, we determined that acid adaptation triggers a degradation of AE2 protein. Since extracellular acidosis did not affect *SLC4A2* mRNA levels, this adaptive mechanism would have been overlooked by transcriptomic methods. We also established that the link between acidosis and AE2 degradation involves the mTOR pathway and lysosomes. AE2 degradation has been reported before,[50,51] but its physiological trigger had not been described. The effect of acidity on inhibiting mTORC1[40,43,52,53] and lysosomal function is well established,[20,43] but its link to AE2 had not been demonstrated. Our study links mTORC1 activity to pHi control via lysosomal-dependent AE2 degradation. We found that blocking lysosomal activity with bafilomycin A1 stabilized AE2 protein and reversed the acid-adaptation effect on pHi. Consistent with our model, the robust effect of bafilomycin A1 on pHi was absent in cells with genetically inactivated *SLC4A2*. Inhibitors of autophagy (e.g., CQ) did not

phenocopy the actions of bafilomycin A1, indicating that acid-evoked AE2 internalization involves an autophagosome-independent form of endocytosis.

The loss of AE2 activity is beneficial in acidic environments because it raises pHi to the physiological range. However, loss of AE2 activity in cells at pHe 7.4 would raise pHi excessively. This overshoot may explain reports of very high pHi in cancer cells,[47,54] arising when pHi measurements are made at normal pHe immediately following a period of acid adaptation. Excessive alkalization may explain why loss of AE2 was found to suppress the growth of ovarian cancer cells, presumably at pHe 7.4.[55] We found that CRC cells with genetically ablated AE2 have a growth disadvantage at physiological pHe, but not in acidic environments. The lack of a growth effect at low pHe is seen because AE2 would normally undergo degradation under acidic conditions; thus both wild-type and AE2-null cells would have similarly low AE2 levels.

Since acid adaptation is a major survival mechanism in cancer, specifically inhibiting degradation of surface-expressed AE2 may have therapeutic value. Bafilomycin A1 treatment will trigger a myriad of cellular responses, which will include AE2 stabilization and cytoplasmic acidification. Selectively blocking plasmalemmal AE2 degradation is desirable, but challenging. This ambition may require further insight into the mechanism that recruits AE2 for lysosomal degradation. Recent studies suggest that ubiquitination could mark specific membrane-bound proteins that become internalized through endocytosis followed by lysosomal degradation.[56] Inhibiting endocytosis may provide a more targeted approach for blocking AE2 degradation therapeutically. Given the recent development of lysosome-targeting chimeras for the degradation of membrane proteins,[57,58] it may also be possible to develop molecules that inhibit the binding of a cell-surface lysosome-shuttling receptor and the extracellular domain of the target protein.

In summary, we have identified lysosomal degradation of surface-expressed AE2 as the principal mechanism for raising pHi in cancer cells adapted to tumor acidity. Targeting pHi control by interfering with AE2 degradation is a promising research avenue, with therapeutic potential for many types of malignancies.

Limitations of the study

More specific approaches will be needed to fully assess the consequences of AE2 stability at the surface membrane. As bafilomycin A1 treatment will have a myriad of effects on multiple proteins, we were unable to determine the consequences of selectively blocking AE2 degradation. It is worth pointing out that AE2 is not the only acid-loading AE targeted by lysosomal degradation. We observed a degradation of AE3 protein in some cell lines following acid adaptation, which may provide an additional means of reducing acid loading. Therefore, studies should focus on reversing degradation of both AE2 and AE3. To that end, it would be interesting to investigate whether specifically blocking AE2 degradation could affect tumor metabolism and metastasis in animal experiments. In the absence of selective tools, this experiment is not yet feasible.

STAR★METHODS

Detailed methods are provided in the online version of this paper and include the following:

- KEY RESOURCES TABLE
- RESOURCE AVAILABILITY
  - Lead contact
  - Materials availability
  - Data and code availability
- EXPERIMENTAL MODEL AND SUBJECT PARTICIPANT DETAILS
  - Cell lines and culture conditions
  - Animals
- METHOD DETAILS
  - Setting and measuring medium pH
  - Intracellular pH measurements
  - Microarray gene expression analysis
  - Statistical analysis of pHi-pHe data and correlation with mRNA expression data
  - Fluorescence-activated cell sorting
  - siRNA transfections
  - Treatment with low chloride- and HEPES/MES-containing media
  - Immunoblotting
  - Cell growth analysis using sulphorhodamine B (SRB)
  - qPCR
  - Medium pH and oxygen usage monitoring using fluorimetric assay
  - Immunoprecipitation
  - Drug treatments
  - Immunofluorescence
  - Anion exchanger activity measurements
  - CRISPR/Cas9-mediated gene knock-out
  - Lysotracker measurements
  - Histology of human tissue sections and mouse xenograft tumors
- QUANTIFICATION AND STATISTICAL ANALYSIS
  - Survival curve fitting

SUPPLEMENTAL INFORMATION

Supplemental information can be found online at https://doi.org/10.1016/j.celrep.2023.112601.

ACKNOWLEDGMENTS

We thank Dr. Ryan Beveridge (MRC Weatherall Institute for Molecular Medicine) for preparing lentivirus samples. This work was supported by the European Research Council (SURVIVE #723997).

AUTHOR CONTRIBUTIONS

J.M., S.M., B.W., A.H., W.B., G.A., E.B., and Z.Y. performed experiments. W.F.B. provided cell lines and advised the analysis. J.M. and P.S. designed the research. J.M. and P.S. wrote the paper.

DECLARATION OF INTERESTS

The authors declare no competing interests.

INCLUSION AND DIVERSITY

We support inclusive, diverse, and equitable conduct of research.

Received: November 22, 2022
Revised: March 16, 2023
Accepted: May 19, 2023
Published: June 3, 2023

REFERENCES

1. Corbet, C., and Feron, O. (2017). Tumour acidosis: from the passenger to the driver's seat. Nat. Rev. Cancer *17*, 577–593. https://doi.org/10.1038/nrc.2017.77.
2. Boedtkjer, E., and Pedersen, S.F. (2020). The acidic tumor microenvironment as a driver of cancer. Annu. Rev. Physiol. *82*, 103–126. https://doi.org/10.1146/annurev-physiol-021119-034627.
3. Estrella, V., Chen, T., Lloyd, M., Wojtkowiak, J., Cornnell, H.H., Ibrahim-Hashim, A., Bailey, K., Balagurunathan, Y., Rothberg, J.M., Sloane, B.F., et al. (2013). Acidity generated by the tumor microenvironment drives local invasion. Cancer Res. *73*, 1524–1535. https://doi.org/10.1158/0008-5472.CAN-12-2796.
4. Casey, J.R., Grinstein, S., and Orlowski, J. (2010). Sensors and regulators of intracellular pH. Nat. Rev. Mol. Cell Biol. *11*, 50–61. https://doi.org/10.1038/nrm2820.
5. Andersen, H.B., Ialchina, R., Pedersen, S.F., and Czaplinska, D. (2021). Metabolic reprogramming by driver mutation-tumor microenvironment interplay in pancreatic cancer: new therapeutic targets. Cancer Metastasis Rev. *40*, 1093–1114. https://doi.org/10.1007/s10555-021-10004-4.
6. Blaszczak, W., Williams, H., and Swietach, P. (2022). Autoregulation of H(+)/lactate efflux prevents monocarboxylate transport (MCT) inhibitors from reducing glycolytic lactic acid production. Br. J. Cancer *127*, 1365–1377. https://doi.org/10.1038/s41416-022-01910-7.
7. Zhang, X., Lin, Y., and Gillies, R.J. (2010). Tumor pH and its measurement. J. Nucl. Med. *51*, 1167–1170. https://doi.org/10.2967/jnumed.109.068981.
8. Gillies, R.J., Raghunand, N., Karczmar, G.S., and Bhujwalla, Z.M. (2002). MRI of the tumor microenvironment. J. Magn. Reson. Imaging. *16*, 430–450. https://doi.org/10.1002/jmri.10181.
9. Lagadic-Gossmann, D., Huc, L., and Lecureur, V. (2004). Alterations of intracellular pH homeostasis in apoptosis: origins and roles. Cell Death Differ. *11*, 953–961. https://doi.org/10.1038/sj.cdd.4401466.
10. Matsuyama, S., Llopis, J., Deveraux, Q.L., Tsien, R.Y., and Reed, J.C. (2000). Changes in intramitochondrial and cytosolic pH: early events that modulate caspase activation during apoptosis. Nat. Cell Biol. *2*, 318–325. https://doi.org/10.1038/35014006.
11. Gatenby, R.A., Gawlinski, E.T., Gmitro, A.F., Kaylor, B., and Gillies, R.J. (2006). Acid-mediated tumor invasion: a multidisciplinary study. Cancer Res. *66*, 5216–5223. https://doi.org/10.1158/0008-5472.CAN-05-4193.
12. Frantz, C., Barreiro, G., Dominguez, L., Chen, X., Eddy, R., Condeelis, J., Kelly, M.J.S., Jacobson, M.P., and Barber, D.L. (2008). Cofilin is a pH sensor for actin free barbed end formation: role of phosphoinositide binding. J. Cell Biol. *183*, 865–879. https://doi.org/10.1083/jcb.200804161.
13. Pope, B.J., Zierler-Gould, K.M., Kühne, R., Weeds, A.G., and Ball, L.J. (2004). Solution structure of human cofilin: actin binding, pH sensitivity, and relationship to actin-depolymerizing factor. J. Biol. Chem. *279*, 4840–4848. https://doi.org/10.1074/jbc.M310148200.
14. Pouysségur, J., Marchiq, I., Parks, S.K., Durivault, J., Ždralević, M., and Vucetic, M. (2022). 'Warburg effect' controls tumor growth, bacterial, viral infections and immunity - genetic deconstruction and therapeutic perspectives. Semin. Cancer Biol. *86*, 334–346. https://doi.org/10.1016/j.semcancer.2022.07.004.
15. White, K.A., Kisor, K., and Barber, D.L. (2019). Intracellular pH dynamics and charge-changing somatic mutations in cancer. Cancer Metastasis Rev. *38*, 17–24. https://doi.org/10.1007/s10555-019-09791-8.
16. White, K.A., Ruiz, D.G., Szpiech, Z.A., Strauli, N.B., Hernandez, R.D., Jacobson, M.P., and Barber, D.L. (2017). Cancer-associated arginine-to-histidine mutations confer a gain in pH sensing to mutant proteins. Sci. Signal. *10*, eaam9931. https://doi.org/10.1126/scisignal.aam9931.
17. Michl, J., Park, K.C., and Swietach, P. (2019). Evidence-based guidelines for controlling pH in mammalian live-cell culture systems. Commun. Biol. *2*, 144. https://doi.org/10.1038/s42003-019-0393-7.
18. Boron, W.F. (2004). Regulation of intracellular pH. Adv. Physiol. Educ. *28*, 160–179. https://doi.org/10.1152/advan.00045.2004.
19. Thomas, R.C. (1989). Cell growth factors. Bicarbonate and pHi response. Nature *337*, 601. https://doi.org/10.1038/337601a0.
20. Damaghi, M., Tafreshi, N.K., Lloyd, M.C., Sprung, R., Estrella, V., Wojtkowiak, J.W., Morse, D.L., Koomen, J.M., Bui, M.M., Gatenby, R.A., and Gillies, R.J. (2015). Chronic acidosis in the tumour microenvironment selects for overexpression of LAMP2 in the plasma membrane. Nat. Commun. *6*, 8752. https://doi.org/10.1038/ncomms9752.
21. Galenkamp, K.M.O., Sosicka, P., Jung, M., Recouvreux, M.V., Zhang, Y., Moldenhauer, M.R., Brandi, G., Freeze, H.H., and Commisso, C. (2020). Golgi acidification by NHE7 regulates cytosolic pH homeostasis in pancreatic cancer cells. Cancer Discov. *10*, 822–835. https://doi.org/10.1158/2159-8290.CD-19-1007.
22. Halestrap, A.P., and Wilson, M.C. (2012). The monocarboxylate transporter family–role and regulation. IUBMB Life *64*, 109–119. https://doi.org/10.1002/iub.572.
23. Koukourakis, M.I., Giatromanolaki, A., Harris, A.L., and Sivridis, E. (2006). Comparison of metabolic pathways between cancer cells and stromal cells in colorectal carcinomas: a metabolic survival role for tumor-associated stroma. Cancer Res. *66*, 632–637. https://doi.org/10.1158/0008-5472.can-05-3260.
24. Hulikova, A., Vaughan-Jones, R.D., and Swietach, P. (2011). Dual role of CO2/HCO3− buffer in the regulation of intracellular pH of three-dimensional tumor growths. J. Biol. Chem. *286*, 13815–13826. https://doi.org/10.1074/jbc.M111.219899.
25. McIntyre, A., Hulikova, A., Ledaki, I., Snell, C., Singleton, D., Steers, G., Seden, P., Jones, D., Bridges, E., Wigfield, S., et al. (2016). Disrupting hypoxia-induced bicarbonate transport acidifies tumor cells and suppresses tumor growth. Cancer Res. *76*, 3744–3755. https://doi.org/10.1158/0008-5472.Can-15-1862.
26. Romero, M.F., Chen, A.P., Parker, M.D., and Boron, W.F. (2013). The SLC4 family of bicarbonate (HCO_3^-) transporters. Mol. Aspects Med. *34*, 159–182. https://doi.org/10.1016/j.mam.2012.10.008.
27. Alper, S.L. (2006). Molecular physiology of SLC4 anion exchangers. Exp. Physiol. *91*, 153–161. https://doi.org/10.1113/expphysiol.2005.031765.
28. Blaszczak, W., and Swietach, P. (2021). What do cellular responses to acidity tell us about cancer? Cancer Metastasis Rev. *40*, 1159–1176. https://doi.org/10.1007/s10555-021-10005-3.
29. Liu, Y., Yang, J., and Chen, L.-M. (2015). Structure and function of SLC4 family HCO3- transporters. Front. Physiol. *6*, 355. https://doi.org/10.3389/fphys.2015.00355.
30. Khosrowabadi, E., Rivinoja, A., Risteli, M., Tuomisto, A., Salo, T., Mäkinen, M.J., and Kellokumpu, S. (2021). SLC4A2 anion exchanger promotes tumour cell malignancy via enhancing net acid efflux across golgi membranes. Cell. Mol. Life Sci. *78*, 6283–6304. https://doi.org/10.1007/s00018-021-03890-y.
31. Thomas, J.A., Buchsbaum, R.N., Zimniak, A., and Racker, E. (1979). Intracellular pH measurements in Ehrlich ascites tumor cells utilizing spectroscopic probes generated in situ. Biochemistry *18*, 2210–2218.
32. Gatenby, R.A., Gillies, R.J., and Brown, J.S. (2010). The evolutionary dynamics of cancer prevention. Nat. Rev. Cancer *10*, 526–527. https://doi.org/10.1038/nrc2892.

33. Flinck, M., Kramer, S.H., Schnipper, J., Andersen, A.P., and Pedersen, S.F. (2018). The acid-base transport proteins NHE1 and NBCn1 regulate cell cycle progression in human breast cancer cells. Cell Cycle *17*, 1056–1067. https://doi.org/10.1080/15384101.2018.1464850.

34. Putney, L.K., and Barber, D.L. (2003). Na-H exchange-dependent increase in intracellular pH times G2/M entry and transition. J. Biol. Chem. *278*, 44645–44649. https://doi.org/10.1074/jbc.M308099200.

35. Liu, T.-C., Kalugin, P.N., Wilding, J.L., and Bodmer, W.F. (2022). GMMchi: gene expression clustering using Gaussian mixture modeling. Preprint at bioRxiv. https://doi.org/10.1101/2022.02.14.480329.

36. Holappa, K., Muñoz, M.T., Egea, G., and Kellokumpu, S. (2004). The AE2 anion exchanger is necessary for the structural integrity of the Golgi apparatus in mammalian cells. FEBS Lett. *564*, 97–103. https://doi.org/10.1016/S0014-5793(04)00315-1.

37. Holappa, K., and Kellokumpu, S. (2003). Targeting of the AE2 anion exchanger to the Golgi apparatus is cell type-dependent and correlates with the expression of Ank(195), a Golgi membrane skeletal protein. FEBS Lett. *546*, 257–264. https://doi.org/10.1016/s0014-5793(03)00597-0.

38. Russell, S., Xu, L., Kam, Y., Abrahams, D., Ordway, B., Lopez, A.S., Bui, M.M., Johnson, J., Epstein, T., Ruiz, E., et al. (2022). Proton export upregulates aerobic glycolysis. BMC Biol. *20*, 163. https://doi.org/10.1186/s12915-022-01340-0.

39. McBrian, M.A., Behbahan, I.S., Ferrari, R., Su, T., Huang, T.-W., Li, K., Hong, C.S., Christofk, H.R., Vogelauer, M., Seligson, D.B., and Kurdistani, S.K. (2013). Histone acetylation regulates intracellular pH. Mol. Cell *49*, 310–321. https://doi.org/10.1016/j.molcel.2012.10.025.

40. Wojtkowiak, J.W., Rothberg, J.M., Kumar, V., Schramm, K.J., Haller, E., Proemsey, J.B., Lloyd, M.C., Sloane, B.F., and Gillies, R.J. (2012). Chronic autophagy is a cellular adaptation to tumor acidic pH microenvironments. Cancer Res. *72*, 3938–3947. https://doi.org/10.1158/0008-5472.CAN-11-3881.

41. Sardiello, M., Palmieri, M., di Ronza, A., Medina, D.L., Valenza, M., Gennarino, V.A., Di Malta, C., Donaudy, F., Embrione, V., Polishchuk, R.S., et al. (2009). A gene network regulating lysosomal biogenesis and function. Science *325*, 473–477. https://doi.org/10.1126/science.1174447.

42. Mauthe, M., Orhon, I., Rocchi, C., Zhou, X., Luhr, M., Hijlkema, K.J., Coppes, R.P., Engedal, N., Mari, M., and Reggiori, F. (2018). Chloroquine inhibits autophagic flux by decreasing autophagosome-lysosome fusion. Autophagy *14*, 1435–1455. https://doi.org/10.1080/15548627.2018.1474314.

43. Walton, Z.E., Patel, C.H., Brooks, R.C., Yu, Y., Ibrahim-Hashim, A., Riddle, M., Porcu, A., Jiang, T., Ecker, B.L., Tameire, F., et al. (2018). Acid suspends the circadian clock in hypoxia through inhibition of mTOR. Cell *174*, 72–87.e32. https://doi.org/10.1016/j.cell.2018.05.009.

44. Walton, Z.E., Brooks, R.C., and Dang, C.V. (2019). mTOR senses intracellular pH through lysosome dispersion from RHEB. Bioessays *41*, e1800265. https://doi.org/10.1002/bies.201800265.

45. Ali, E.S., Lipońska, A., O'Hara, B.P., Amici, D.R., Torno, M.D., Gao, P., Asara, J.M., Yap, M.-N.F., Mendillo, M.L., and Ben-Sahra, I. (2022). The mTORC1-SLC4A7 axis stimulates bicarbonate import to enhance de novo nucleotide synthesis. Mol. Cell *82*, 3284–3298.e7. https://doi.org/10.1016/j.molcel.2022.06.008.

46. Swietach, P. (2019). What is pH regulation, and why do cancer cells need it? Cancer Metastasis Rev. *38*, 5–15. https://doi.org/10.1007/s10555-018-09778-x.

47. Webb, B.A., Chimenti, M., Jacobson, M.P., and Barber, D.L. (2011). Dysregulated pH: a perfect storm for cancer progression. Nat. Rev. Cancer *11*, 671–677. https://doi.org/10.1038/nrc3110.

48. Pandey, R., Zhou, M., Islam, S., Chen, B., Barker, N.K., Langlais, P., Srivastava, A., Luo, M., Cooke, L.S., Weterings, E., and Mahadevan, D. (2019). Carcinoembryonic antigen cell adhesion molecule 6 (CEACAM6) in Pancreatic Ductal Adenocarcinoma (PDA): an integrative analysis of a novel therapeutic target. Sci. Rep. *9*, 18347. https://doi.org/10.1038/s41598-019-54545-9.

49. Olive, P.L., Aquino-Parsons, C., MacPhail, S.H., Liao, S.Y., Raleigh, J.A., Lerman, M.I., and Stanbridge, E.J. (2001). Carbonic anhydrase 9 as an endogenous marker for hypoxic cells in cervical cancer. Cancer Res. *61*, 8924–8929.

50. Wang, T., Fei, H.-J., Yang, Y., Jiang, X.-S., Yan, M., Zeng, Z., Wu, J., Song, L.-J., Tian, H., and Fu, G.-H. (2016). Expression of AE1/p16 promoted degradation of AE2 in gastric cancer cells. BMC Cancer *16*, 716. https://doi.org/10.1186/s12885-016-2751-x.

51. Itoh, R., Hatano, N., Murakami, M., Mitsumori, K., Kawasaki, S., Wakagi, T., Kanzaki, Y., Kojima, H., Kawaai, K., Mikoshiba, K., et al. (2021). Both IRBIT and long-IRBIT bind to and coordinately regulate Cl(-)/HCO(3)(-) exchanger AE2 activity through modulating the lysosomal degradation of AE2. Sci. Rep. *11*, 5990. https://doi.org/10.1038/s41598-021-85499-6.

52. Faes, S., Duval, A.P., Planche, A., Uldry, E., Santoro, T., Pythoud, C., Stehle, J.C., Horlbeck, J., Letovanec, I., Riggi, N., et al. (2016). Acidic tumor microenvironment abrogates the efficacy of mTORC1 inhibitors. Mol. Cancer *15*, 78. https://doi.org/10.1186/s12943-016-0562-y.

53. Balgi, A.D., Diering, G.H., Donohue, E., Lam, K.K.Y., Fonseca, B.D., Zimmerman, C., Numata, M., and Roberge, M. (2011). Regulation of mTORC1 Signaling by pH. PLoS One *6*, e21549. https://doi.org/10.1371/journal.pone.0021549.

54. Gallagher, F.A., Kettunen, M.I., Day, S.E., Hu, D.-E., Ardenkjær-Larsen, J.H., Zandt, R.i.t., Jensen, P.R., Karlsson, M., Golman, K., Lerche, M.H., and Brindle, K.M. (2008). Magnetic resonance imaging of pH in vivo using hyperpolarized 13C-labelled bicarbonate. Nature *453*, 940–943. https://doi.org/10.1038/nature07017.

55. Zhang, L.-J., Lu, R., Song, Y.-N., Zhu, J.-Y., Xia, W., Zhang, M., Shao, Z.-Y., Huang, Y., Zhou, Y., Zhang, H., et al. (2017). Knockdown of anion exchanger 2 suppressed the growth of ovarian cancer cells via mTOR/p70S6K1 signaling. Sci. Rep. *7*, 6362. https://doi.org/10.1038/s41598-017-06472-w.

56. Clague, M.J., and Urbé, S. (2010). Ubiquitin: same molecule, different degradation pathways. Cell *143*, 682–685. https://doi.org/10.1016/j.cell.2010.11.012.

57. Banik, S.M., Pedram, K., Wisnovsky, S., Ahn, G., Riley, N.M., and Bertozzi, C.R. (2020). Lysosome-targeting chimaeras for degradation of extracellular proteins. Nature *584*, 291–297. https://doi.org/10.1038/s41586-020-2545-9.

58. Békés, M., Langley, D.R., and Crews, C.M. (2022). PROTAC targeted protein degraders: the past is prologue. Nat. Rev. Drug Discov. *21*, 181–200. https://doi.org/10.1038/s41573-021-00371-6.

59. Sanjana, N.E., Shalem, O., and Zhang, F. (2014). Improved vectors and genome-wide libraries for CRISPR screening. Nat. Methods *11*, 783–784. https://doi.org/10.1038/nmeth.3047.

60. Blaszczak, W., Tan, Z., and Swietach, P. (2021). Cost-effective real-time metabolic profiling of cancer cell lines for plate-based assays. Chemosensors *9*, 139.

STAR★METHODS

KEY RESOURCES TABLE

REAGENT or RESOURCE	SOURCE	IDENTIFIER
Antibodies		
Rabbit polyclonal anti-AE2 (used for Western Blotting)	Novus Biologicals	NBP2-15301
Rabbit polyclonal anti-AE2 (used for immunofluorescence)	Novus Biologicals	NBP2-92513
Rabbit polyclonal anti-SLC4A3	Invitrogen	PA5-51351; RRID: AB_2636798
Mouse monoclonal anti-SLC26A3	Santa Cruz	sc-376187; RRID: AB_10990725
Mouse monoclonal anti-SLC26A6	Santa Cruz	sc-515230
Rabbit polyclonal anti-NDUFS1	Invitrogen	PA5-22309; RRID: AB_11151879
Rabbit polyclonal anti-LC3	Invitrogen	PA1-16931; RRID: AB_2137583
Mouse monoclonal anti-LAMP2	Santa Cruz	Sc-18822; RRID AB_626858
Phospho-mTOR (S2481)	Cell signalling	#2974P
Anti-phospho-S6 (Ser240/244)	Cell signalling	#5364P
Anti-phospho-EIF3 (S422)	Cell signalling	#3591P
Anti-phospho-S6K (T389)	Cell signalling	#9234P
S6K	Cell signalling	#2708P
HRP-conjugated anti-β-actin	Proteintech	HRP-60008; RRID: AB_2819183
Mouse monoclonal anti-ubiquitin	Invitrogen	13-1600; RRID: AB_2533002
Mouse monoclonal anti-EPCAM	In-house, Bodmer Lab (Weatherall Institute of Molecular Medicine, University of Oxford)	N/A
Mouse monoclonal anti-GM130	BD Biosciences	610822; RRID:AB_610822
Goat anti-Mouse IgG (H+L) Highly Cross-Adsorbed Secondary Antibody, Alexa Fluor™ Plus 555	Invitrogen	A32727; RRID:AB_2633276
Goat anti-Rabbit IgG (H+L) Highly Cross-Adsorbed Secondary Antibody, Alexa Fluor™ Plus 488	Invitrogen	A32731; RRID:AB_2633280
Bacterial and virus strains		
5-alpha Competent *E. coli* (High Efficiency)	New England Biolabs	C2987H
Chemicals, peptides and recombinant proteins		
DMEM	Life technologies,	41965-039
Sodium bicarbonate-free DMEM	Sigma-Aldrich	D7777
Sodium bicarbonate, glucose and phenol red-free DMEM	Sigma-Aldrich	D5030
Foetal Bovine Serum	Merck Life Science	F9665-500ML
Penicillin-Streptomycin	Sigma-Aldrich	P0781
Sodium bicarbonate	Sigma-Aldrich	S5761
Sodium chloride	Sigma-Aldrich	S5653
Glutamine	Sigma-Aldrich	G7513
Polybrene	Merck Life Science	H9268-5G
Puromycin	Santa Cruz	sc-108071A
Sulphorhodamine B	Sigma-Aldrich	230162-5G
Trichloroacetic acid	Merck Life Science	91230-100G

(*Continued on next page*)

Continued

REAGENT or RESOURCE	SOURCE	IDENTIFIER
Acetic acid	Sigma-Aldrich	A6283-500ML
Tris Base	Sigma-Aldrich	T1503-1KG
Radioimmunoprecipitation assay (RIPA) buffer	Cell Signalling	9806S
Acrylamide	Geneflow Ltd	A2-0074
8-Hydroxypyrene-1,3,6-trisulfonic acid trisodium salt (HPTS)	Sigma-Aldrich	H1529
Tris(bipyridine)ruthenium(II) chloride (RuBPY)	Sigma-Aldrich	224758
Sodium pyruvate	Gibco	11360-070
Sodium gluconate	Sigma-Aldrich	822058
HEPES	Sigma-Aldrich	H3375
MES	Sigma-Aldrich	M3671
D-(+)-Glucose	Sigma-Aldrich	G7021-1KG
Hoechst 33342	Invitrogen	H3570
5-(and-6)-carboxy SNARF-1 acetoxymethyl ester, acetate	Invitrogen	C1272
cariporide	Tocris	5358
MG-132	Cambridge Biosciences	HY-13259-10mg
Matrigel	Corning	356234
A-485	Tocris	**6387**
Lysotracker green DND-26	Invitrogen	L7526
Bafilomycin A1	Sigma-Aldrich	B1793
Glycyl-L-phenylalanine 2-naphthylamide (GPN)	Bachem AG	K-1325
Chloroquine	Alfa Aesar	J64459
Rapamycin	Cell guidance systems	SM83-5
TaqMan master mix	Applied Biosystems	4304437
TaqMan probe SLC4A2	Life Technologies	4448489
Taqman probe Actin	Applied Biosystems	4333762F
Protein A/G magnetic agarose beads	Pierce	78609
Cycloheximide	Santa Cruz Biotechnology	Sc-3508B
Critical commercial assays		
QIAquick Gel Extraction Kit	QIAGEN	28706X4
Bicinchoninic acid (BCA) protein assay kit	Thermo Fisher Scientific	23225
iScript cDNA Synthesis script	Bio-Rad	1708891
RNeasy Kit	QIAGEN	74104
Deposited data		
Supplementary code 1 and 2	This paper	Mendeley https://doi.org/10.17632/n8hp45bdrj.1
Supplementary code 3 and 4	This paper	Mendeley https://doi.org/10.17632/68crc9wf39.1
Supplementary code 5	This paper	Mendeley https://doi.org/10.17632/cw4b9tjygj.1
Experimental models: Cell lines		
Human: C10	Walter Bodmer's laboratory (WBL), University of Oxford	N/A

(*Continued on next page*)

Continued

REAGENT or RESOURCE	SOURCE	IDENTIFIER
Human: C106	WBL	N/A
Human: C2BBE1	WBL	N/A
Human: C32	WBL	N/A
Human: C99	WBL	N/A
Human: CACO2	WBL	N/A
Human: CAR1	WBL	N/A
Human: CC20	WBL	N/A
Human: CCK81	WBL	N/A
Human: CCO7	WBL	N/A
Human: CL40	WBL	N/A
Human: COLO205	WBL	N/A
Human: COLO206	WBL	N/A
Human: COLO320DM	WBL	N/A
Human: COLO320HSR	WBL	N/A
Human: COLO678	WBL	N/A
Human: CX1	WBL	N/A
Human: DLD1	WBL	N/A
Human: GP2D	WBL	N/A
Human: GP5D	WBL	N/A
Human: HCC2998	WBL	N/A
Human: HCC56	WBL	N/A
Human: HCT116	WBL	N/A
Human: HCT15	WBL	N/A
Human: HDC111	WBL	N/A
Human: HDC114	WBL	N/A
Human: HDC54	WBL	N/A
Human: HDC57	WBL	N/A
Human: HDC82	WBL	N/A
Human: HDC9	WBL	N/A
Human: HRA19	WBL	N/A
Human: HT29	WBL	N/A
Human: HT55	WBL	N/A
Human: JHCOLOY1	WBL	N/A
Human: LOVO	WBL	N/A
Human: LS180	WBL	N/A
Human: LS411	WBL	N/A
Human: LS513	WBL	N/A
Human: NCIH508	WBL	N/A
Human: NCIH548	WBL	N/A
Human: NCIH747	WBL	N/A
Human: OUMS23	WBL	N/A
Human: OXCO2	WBL	N/A
Human: PMFKO14	WBL	N/A
Human: RCM1	WBL	N/A
Human: RKO	WBL	N/A
Human: RW2982	WBL	N/A
Human: RW7213	WBL	N/A
Human: SKCO1	WBL	N/A
Human: SNU1235	WBL	N/A
Human: SNUC1	WBL	N/A
Human: SNUC2B	WBL	N/A
Human: SW1222	WBL	N/A
Human: SW1417	WBL	N/A
Human: SW403	WBL	N/A
Human: SW48	WBL	N/A
Human: SW480	WBL	N/A
Human: SW620	WBL	N/A
Human: SW837	WBL	N/A
Human: SW948	WBL	N/A

(*Continued on next page*)

Continued

REAGENT or RESOURCE	SOURCE	IDENTIFIER
Human: VACO10MS	WBL	N/A
Human: VACO4A	WBL	N/A
Human: VACO4S	WBL	N/A
Human: VACO5	WBL	N/A
Human: MIA Pa-Ca-2	Prof. Alessandra Fiorio, University of Lille, France	N/A
Human PANC-1	Prof. Anna Trauzold, University of Kiel, Germany	N/A
Experimental models: Organisms/strains		
Female athymic Nude Crl:NU(NCr)-Foxn1nu mice	Charles River	N/A
Biological samples		
Matched Pair – Paraffin Tissue Section	BioChain	T8235090
Oligonucleotides		
LentiCRISPR sgSLC4A2 AAGAATCTGCGCCCTTGGCG	Invitrogen	N/A
LentiCRISPR sgNDUFS1 TAGAATGTATGCCTACTTGG	Invitrogen	N/A
siGENOME siControl	Dharmacon	D-001210-01-05
siGENOME siBNIP3	Dharmacon	M-004636-01-0005
siGENOME siPEG10	Dharmacon	M-032579-01-0005
siGENOME siSLC16A7	Dharmacon	M-007409-01-0005
siGENOME siATP6V0A2	Dharmacon	M-019950-00-0005
siGENOME siCEACAM6	Dharmacon	M-015306-01-0005
siGENOME siPMP22	Dharmacon	M-010616-02-0005
siGENOME siCA9	Dharmacon	M-005244-02-0005
siGENOME siSLC4A2	Dharmacon	M-007582-01-0005
siGENOME siSLC4A3	Dharmacon	M-007583-02-0005
siGENOME siSLC26A3	Dharmacon	M-007492-00-0005
siGENOME siSLC26A6	Dharmacon	M-007494-01-0005
siGENOME siTFEB	Dharmacon	M-009798-02-0005
siGENOME ATG5	Dharmacon	M-004374-04-0005
Recombinant DNA		
lentiCRISPR v2	Sanjana et al., 2014[59]	Addgene: 52961
lentiCRISPR constructs with gRNA insert listed above		In this paper
Software and algorithms		
Fiji	ImageJ	N/A
Gen5 v.10	Biotek	N/A
MATLAB R2020b	Mathworks	N/A

RESOURCE AVAILABILITY

Lead contact

Further information and requests for resources and reagents should be directed to and will be fulfilled by the lead contact, Pawel Swietach (pawel.swietach@dpag.ox.ac.uk).

Materials availability

Plasmids generated in this study are available upon request from the lead contact.

Data and code availability

- This paper does not contain any standardized datasets. All data reported in this paper will be shared by the lead contact upon request.

- All original code has been deposited at Mendeley and is publicly available as of the date of publication. DOIs are listed in the key resources table.
- Any additional information required to reanalyze the data reported in this paper is available from the lead contact upon request.

EXPERIMENTAL MODEL AND SUBJECT PARTICIPANT DETAILS

Cell lines and culture conditions

Human colorectal cells (listed under Key Resources) were obtained from Prof. Walter Bodmer's collection at the Weatherall Institute of Molecular Medicine (University of Oxford, UK). Cell lines were cultivated in DMEM (Gibco 41965-039), supplemented with 10% FBS (Sigma-Aldrich) and 1% PS (100 U mL^{-1} penicillin, 100 μg mL^{-1} streptomycin; Sigma-Aldrich). For pHi measurements, cells were treated with media based on $NaHCO_3$-free DMEM (Sigma-Aldrich, Cat. No. D7777), supplemented with 10% FBS, 1 % PS and various concentrations of $NaHCO_3$ and NaCl, to achieve desired/calculated pHe values at 5% CO_2, as indicated in figure legends. In addition, $NaHCO_3$-free, glucose-free and phenol red-free DMEM (Sigma-Aldrich, Cat. No. D5030) supplemented with 10% FBS, 1 % PS, 25 mM glucose and various $NaHCO_3$ and NaCl concentrations, as indicated in figure legends was used. Cells were maintained at 37 °C and 5% CO_2. Lines were authenticated by single nucleotide polymorphism (SNP)-based profiling and tested routinely for mycoplasma contamination.

Animals

Female athymic Nude Crl:NU(NCr)-Foxn1nu mice were 12 weeks old before subcutaneous injection with either SW1222 WT or COLO320HSR cells. Cells were resuspended in 100 μL of a 1:1 mixture of matrigel and serum-free DMEM medium before injection. Each mouse was injected with 2 million SW1222 WT cells on the left flank and 2 million COLO320 HSR cells on the right flank. All animal procedures were carried out in accordance with national and institutional guidelines, with the approval of ethics and welfare board instructions, and with the authority of Home Office Project Licence PPL P01A04016.

METHOD DETAILS

Setting and measuring medium pH

Media were prepared by mixing NaHCO3-free Dulbecco's modified Eagle's medium (DMEM) (Sigma-Aldrich, Cat. No. D7777), supplemented with 10% FBS (Sigma-Aldrich) and 1% penicillin-streptomycin (PS) (100 U/mL penicillin, 100 mL/mL streptomycin; Sigma Aldrich). Medium pH was set by adjusting [HCO_3^-], achieved by mixing various ratios of stocks containing either 44 mM $NaHCO_3$ or 44 mM NaCl. This strategy ensures that osmolarity is constant. Medium pH was measured by Phenol Red absorbance at 430 nm and 560 nm using Cytation 5 imaging plate reader equipped with a CO_2 gas controller (Biotek). Measurement were taken from 200 mL medium in a clear, flat-bottom 96-well plate (Costar) without lids at 37°C

Intracellular pH measurements

pH was measured using cSNARF1 in cell identified by particle analysis of fluorescence centered around nuclei visualized using the DNA-binding stain Hoechst-33342. Cells were plated in triplicate at 50,000-100,000 cells per well in black wall, flat coverslip bottom μ-plate 96-well plates with a growth area of 0.56 cm^2 per well (Ibidi) and were left to attach overnight. They were then incubated in media supplemented with cSNARF1-AM (5 μg/mL, Invitrogen) and the nuclear stain Hoechst-33342 (10 μg/mL, Molecular Probes), for 15 min, and then replaced with medium of varying sodium bicarbonate concentration (twice). Images of fluorescence excited at 377 nm and collected at 447 nm (Hoechst-33342), and of fluorescence excited at 531 nm and collected at 590 nm and 640 nm (cSNARF1), were acquired using Cytation 5 imaging plate reader (Biotek) and its bespoke software. Images were either acquired using a 4x objective, or a 10x objective. Measurements were performed in an atmosphere of 37°C and 5% CO_2, established in the plate reader. Further analysis of the population distribution of pH data was performed using a MATLAB script (Supplementary Code 1). cSNARF1 fluorescence ratios were converted into pH_i using a calibration curve obtained through the nigericin method. pH_i distributions from replicate wells were pooled, and low intensity measurements were removed using a second MATLAB script (Supplementary Code 2).

Microarray gene expression analysis

Total RNA from cells was extracted using the RNeasy kit (Qiagen) according to the manufacturer's instructions. All samples were processed in accordance with the Affymetrix protocol, and 2 μg of fragmented and labeled cDNA was hybridized to the Affymetrix GeneChip U133+2 arrays.

Statistical analysis of pHi-pHe data and correlation with mRNA expression data

For 66 CRC cell lines, average pHi, standard deviation, and number of cells was determined for six different pHe values (from 6.63 to 7.70). Experiments were carried out in triplicate and two to five biological repeats were carried out for each cell line. Linear regression based on pHi at all 6 different pHe values was carried out in MATLAB (Supplementary Code 3). Slope, intercept, resting

pHi (at pHe 7.4), and standard deviation were obtained as an average for multiple biological repeats. Slope was plotted against standard deviation, and k-means clustering was used to classify cell lines into four distinct groups. For detection of differentially expressed genes in cell lines with high or low slope and standard deviations, t-tests and Fisher's exact test were carried out (Supplementary Code 4).

Fluorescence-activated cell sorting

Cells were dissociated and loaded with cSNARF1-AM (10 μg/mL, Molecular Probes) for 10 minutes in M199 medium buffered with 20 mM HEPES and titrated to pH 7.4. After replacing the medium the cells were immediately FACS sorted into the top 10% most acidic cells and the top 10% most alkaline cells. cSNARF1 fluorescence was excited at 561 nm and was collected at 585 nm (15 nm bandwidth) and 640 nm (14 nm bandwidth) on a BD FACSDiva. Cells with a high 585/640 nm ratio were considered acidic, and cells with a low 580/640 nm ratio were considered alkaline.

siRNA transfections

Cells were plated at 200 000 cells/well in a clear, flat bottom 6-well plate in 3 mL DMEM supplemented with 10% FBS and 1% PS. 10 nM Dharmacon smartpool siRNA was resuspended in 300 μL optiMEM. In a separate tube, 6 μL Lipofectamine RNAiMAX transfection reagent were mixed with 300 μL optiMEM. siRNA and transfection reagent mixtures were combined and incubated at room temperature for 10 min. Afterwards, the mixture was added to cells in suspension and incubated for 48 h. Experiments were performed 72 h after siRNA-transfection.

Treatment with low chloride- and HEPES/MES-containing media

pHi was measured in response to treatment with medium containing reduced amounts of chloride or HEPES/MES buffering instead of medium with physiological buffering. Low chloride medium was based on the D5030 formulation, with sodium chloride being replaced with sodium gluconate. HEPES/MES buffered medium was based on D5030, supplemented with 10 mM HEPES and 10 mM MES and 24 mM NaCl. The medium was then titrated to the indicated pHe at 37°C.

Immunoblotting

Samples were prepared by lysing the cells using radioimmunoprecipitation assay (RIPA) buffer containing proteinase and phosphatase inhibitors. Protein concentration in the samples was measured using bicinchoninic acid (BCA) protein assay kit and adjusted using water. Samples were not heated, and loaded onto a 10% acrylamide gel. The gel was run at 90 V for 15 minutes and at 120 V for 90 minutes. Afterwards, membrane transfer was performed at 90 V for 90 minutes. Primary antibodies against SLC4A2, SLC4A3, SLC26A3, SLC26A6, β-Actin, LC3A/LC3B, LAMP2, phospho-mTOR, phospho-S6 (Ser240/244), phospho-EIF4B, phospho-S6K (T384),S6K and ubiquitin were applied overnight. Afterwards, membranes were incubated in either and goat anti-rabbit or anti-mouse secondary antibody (1:5000) were applied, and the membrane was visualized using horseradish peroxidase. Antibody binding of β-Actin protein was used as a loading control. Western blot signals were quantified using the ImageJ Gel Analysis tool.

Cell growth analysis using sulphorhodamine B (SRB)

Cells were plated in triplicate at densities of 2000-4000 cells/well in clear, flat bottom 96-well plates (Costar). The following day, the medium was replaced with 200 μL medium of different sodium bicarbonate concentrations as indicated in figure legends. Cells were cultured for six days and extracellular pH was monitored on each day using phenol red absorbance. After six days, the cells were fixed using 10% trichloroacetic acid (TCA) at 4°C for 60 min. Afterwards they were washed with H_2O four times and stained with SRB (0.057% in 1% acetic acid) for 30 min. Residual SRB was removed by washing four times with 1% acetic acid. SRB was then dissolved in 10 mM Tris base. SRB absorbance was read at 520 nm using Cytation5 imaging plate reader (Biotek).

qPCR

Total cellular RNA was isolated (RNeasy kit, Qiagen, 74104) from cells cultured for 72 h hours in sodium bicarbonate/CO_2 buffered conditions of either pH 7.4 or pH 6.4 in 6-well plates. iScript Advanced cDNA synthesis Kit was used for the reversed transcription reaction into cDNA. The resulting cDNA was diluted 1:10 in DNAse-free water before quantification by real-time PCR. qPCR was carried out using Taqman probes for SLC4A2 and β-Actin. 2x Taqman Fast Advanced Mastermix was used for PCR reactions at standard cycling conditions using Applied Biosystems StepOne System. The transcript levels were normalized with the β-Actin transcript level and data were represented as fold change relative to the average of control samples. Data are representative of at least 5 independent experiments.

Medium pH and oxygen usage monitoring using fluorimetric assay

Cells were cultured at high density (70,000 cells/well) in flat-bottom, black 96-well plates. To report extracellular pH and O_2, media contained 2 mM HPTS (8-Hydroxypyrene-1,3,6-trisulfonic acid trisodium salt) and 50 mM RuBPY (tris(bipyridine)ruthenium(II) chloride), as described previously.[60] Media were based on DMEM (D5030) and contained 25 mM glucose, 10% FBS, 1% PS, 1 mM pyruvate, 1% glutamax and 2 mM HEPES and MES, as indicated. NaCl was added to a concentration that maintains overall osmolarity. Prior to measurements, each well was sealed with 150 μL mineral oil to restrict O_2 ingress. HPTS and RuBPY fluorescence

were monitored for 17 h using a Cytation 5 device (BioTek, Agilent, Winooski, VT, USA). Excitation was provided by a monochromator, and fluorescence emission was detected sequentially at five wavelengths, which were optimized for the dye combination used. Optimal settings on our system were excitation wavelengths of 400, 416, 450, 460, and 540 nm, and the corresponding emissions were 510, 510, 620, 510, and 580 nm.

Immunoprecipitation

DLD1 cells were lysed by scraping cells in a buffer consisting of 50 mM Tris-Hcl, 150 mM NaCl, 1 mM EDTA, 1% triton X-100 and 5% glycerol. Afterwards, we added antibodies for AE2 or ubiquitin the protein lysate (1.2 mg total protein were used) and incubated the mixture overnight at 4°C. The following day, antibody-antigen complexes were added to 100 μL of pre-equilibrated magnetic agarose beads for six hours. Unbound proteins were removed by washing the bead-protein complexes four times in PBS. Protein complexes were eluted from the beads by boiling the samples in 2x Laemmli buffer (containing 10% β-mercapto ethanol) for 5 min. Immunoprecipitated protein complexes were analyzed using western blotting. The obtained membranes incubated with primary antibodies for AE2 and ubiquitin overnight.

Drug treatments

A485, MG132, rapamycin, chloroquine and bafilomycin A1 were dissolved in DMSO. GPN and cycloheximide were dissolved in water. Drugs were stored at -20 degrees and used at concentrations and duration indicated in the figure legends.

Immunofluorescence

For immunofluorescence experiments on cultured cells, cells were cultured in Ibidi 12-well slides as indicated in figure legends. After three days, cells were fixed with 4% paraformaldehyde for 10 minutes at RT. After 10 min of permeabilization with 0.2% Triton X-100, 1 h of blocking with 3% BSA, cells were incubated with primary antibodies for 1.5 – 24 h (Anti-LAMP2 1:250, anti-AE2, anti-GM130 and anti-EPCAM 1:400), followed by secondary antibodies for 1 h (anti-mouse Alexafluor 555, anti-rabbit Alexaflour 488, 1:500) and staining with Hoechst 33342 for 1 min. Slides were mounted with Antifade Gold mounting medium. Images were acquired using a 40x objective on the Zeiss LSM 700 confocal microscope.

Anion exchanger activity measurements

Cells were grown in Ibidi 4-well μ-slide at conditions indicated in figure legends. Prior to measurements, medium was replaced to HEPES-buffered D5030 medium titrated to either pH 7.4 or 6.4. Cells were loaded with cSNARF1 for 10 minutes to report intracellular pH. Solutions were delivered at 37°C to an Ibidi μ-slide. Cells were first equilibrated to Normal Tyrode solution for several minutes before the start of recordings. Intracellular pH measurements were recorded for cells superfused for 1 min in Normal Tyrode (pH 7.4), 6 min in acetate-containing solutions, 3 min in chloride-free solutions, followed by a 5 min recovery period in Normal Tyrode solution. Normal Tyrode contained (in mM) 135 NaCl, 4.5 KCl, 1 $CaCl_2$, 1 $MgCl_2$, 11 glucose, 20 HEPES at pH 7.4. In chloride-free solutions, NaCl was iso-osmotically replaced with sodium gluconate. KCl, $MgCl_2$ and $CaCl_2$ were replaced with potassium gluconate, magnesium gluconate and calcium gluconate, respectively. In acetate-containing solutions, NaCl was iso-osmotically replaced with sodium acetate. Images were acquired using a 40x objective on the Zeiss LSM 700 confocal microscope.

CRISPR/Cas9-mediated gene knock-out

LentiCRISPR v2 was a gift from Feng Zhang (Addgene plasmid # 52961; http://n2t.net/addgene:52961; RRID:Addgene_52961). sgRNA sequences were cloned into LentiCRISPR v.2 backbone using the following protocol: http://genome-engineering.org/gecko/wp-content/uploads/2013/12/lentiCRISPRv2-and-lenti Guide-oligo-cloning-protocol.pdf. Briefly, LentiCRISPR v 2 backbone was digested using BsmBI enzyme for 1 h at 37°C. After gel purification, the linearized DNA was ligated with oligo duplex using the Quick Ligation Kit (NEB M2200S). Plasmid DNA was transformed into DH5alpha competent cells (NEB C2987H).

sgRNA sequences are listed in the key resources table. Virus aliquots were prepared by the Virus Production Facility at WIMM, University of Oxford. DLD1 cells were plated in clear, flat-bottom 6-well plate at a density of 200,000 cells/well and transduced using a 500 mL aliquot of lentivirus carrying the LentiCRISPR v2 construct encoding for a sgRNA sequence targeting *SLC4A2*. Polybrene was added at a concentration of 4 mg/mL. The 6-well plate was incubated for two days before puromycin (5 μg/mL) was added for selection, and cells were incubated for three days before the transduced cells were used for setting up further experiments. Infected cells were seeded at 2 cells/well in 200 mL of media in wells of 96-well plates. Single-cell clones were established and tested for AE2 expression using Western blotting.

Lysotracker measurements

Cells were cultured in Ibidi 4-well μ-slides at conditions indicated in figure legends for three days. Prior to imaging, the medium was replaced with HEPES-buffered D5030 medium titrated to pH 7.4. Lysotracker Green DND 26 and Hoechst33342 were added to the medium at concentration of 100 nM and 10 μg/mL, respectively. After 10 min of incubation, Lysotracker fluorescence was recorded at 488 nm excitation, emission >510 nm using Zeiss LSM 700 confocal microscope. Number of lysosomes per cell and their distance from the nucleus was measured using an in-house MATLAB script (Supplementary Code 5).

Histology of human tissue sections and mouse xenograft tumors

Matched pairs of tumor and normal colon formalin fixed paraffin embedded human tissue (FFPE) sections were obtained from BioChain. The sections were heated for 60°C for 1 h and de-waxed using xylene for 3x 5 min. After rehydration (5 min in 100/90/70% ethanol), slides were washed 3 times in dH_2O. Sections were boiled in 10 mM sodium citrate to achieve antigen unmasking. After permeabilization in 0.1% triton-X100 for 10 min, sections were blocked in 10% FBS in PBS-Tween (0.1%) for 1 h.

Sections were incubated with primary antibodies against AE2 (Novus, NBP2-92513), LAMP2 (Santa Cruz, sc-18822) overnight (1:200 in 3% BSA in PBS-Tween). After incubation with secondary antibodies for 1 h (anti-rabbit Alexafluor 555, anti-mouse Alexafluor 488) and staining with DAPI for 10 min, slides were mounted with Antifade Gold mounting medium. Images were acquired using a 10x and 40x objective on the Zeiss LSM 700 confocal microscope.

Tissues from mouse xenografts were cryo-sectioned. Fresh-frozen sections were first fixed in 10% formalin solution for 3 min. After permeabilization in 0.1% Triton X-100 for 5 min, sections were blocked in 1% mouse serum for 30 min. Sections were incubated with primary antibodies against AE2 (Novus, NBP2-92513), LAMP2 (Santa Cruz, sc-18822) for 1.5 h (1:200 in 3% BSA in PBS-Tween). After incubation with secondary antibodies for 20 min (anti-rabbit Alexafluor 555, anti-mouse Alexafluor 488) slides were mounted with Drop-n-stain mounting medium (containing DAPI). Images were acquired using a 10x objective on the Zeiss LSM 700 confocal microscope.

QUANTIFICATION AND STATISTICAL ANALYSIS

Survival curve fitting

The relationship between cell survival and medium pH for different cell lines and gene knock-outs was analyzed using an in-house script written in Matlab. Data from individual repeats were pooled.

Statistics

Data was analyzed using GraphPad Prism 9. Data are represented expressed as mean ± S.E.M. Data was compared using unpaired t-test, Fisher's exact test, one-way ANOVA or two-way ANOVA. *=P<0.05, **=P<0.01, ***=P<0.001.